Influence of random multi-point seismic excitations on the safety performance of a train running on a long-span bridge

Wei Wang[a,b], Yahui Zhang[a*], Huajiang Ouyang[c]

[a] *State Key Laboratory of Structural Analysis for Industrial Equipment, Department of Engineering Mechanics, International Center for Computational Mechanics, Dalian University of Technology, Dalian 116023, PR China;*

[b] *Technical Center, Shaanxi Automobile Group Co., Ltd., Xi'an 710200, PR China;*

[c] *School of Engineering, University of Liverpool, The Quadrangle, Liverpool L69 3GH, UK*

Corresponding author:

Dr. Y. H. Zhang

State Key Laboratory of Structural Analysis for Industrial Equipment, Department of Engineering Mechanics, Dalian University of Technology, Dalian 116023, PR China

Email: zhangyh@dlut.edu.cn

Tel: +86 411 84706337

Fax: +86 411 84708393

Abstract

The increasing use of bridges in high-speed railway (HSR) lines raises the possibility of train derailment on bridges under seismic excitations. In this paper, the influence of random multi-point earthquakes on the safe running of a train on a long-span bridge is studied in terms of the dynamic reliability, considering spatial seismic effects, and randomness of ground motions and train locations. The equations of motion for the train and the track/bridge as time-invariant subsystems under earthquakes are established, separately. The two subsystems are connected via the wheel-rail interface, for which a nonlinear contact model and detachment are considered. The time-history samples of non-stationary multi-point random earthquakes considering wave passage effects and incoherence effects are generated by the auto regressive moving average (ARMA) model. The ground motions are imposed on the bridge support points in terms of displacement and velocity. The train location at the time of earthquake is considered a uniformly distributed random variable. The running safety reliability of a train moving on a long-span bridge under earthquakes is determined by combining subset simulation (SS) with a prediction-based iterative solution method. Under different seismic components, train speeds, apparent seismic wave velocities and seismic intensities, the most unfavourable train location intervals are determined, which provides a reference for the safety performance assessment of trains travelling on bridges under earthquakes. Numerical results show that the influence of the lateral seismic component on the wheel derailment coefficient (WDC) is greater than the vertical seismic component, and the earthquake that occurs before the train's arrival at 70% length of the bridge will

significantly reduce its running safety.

Keywords: Train-track-bridge system; Wheel-rail contact; Subset simulation; Earthquake; Dynamic reliability

1 Introduction

Because of high smoothness, good stability, small foundation settlement, and easy maintenance, bridges can fulfil the requirements of safe and stable operations of high-speed trains, and hence occupy a large proportion in HSR lines. According to the statistics,[1] bridges account for about 47% of Japan's HSR lines, and the average occupancy rate of bridges in China's HSR exceeds 50%. With the increase of the bridge length in HSR, the possibility of a train derailment on a bridge under earthquakes increases. For example, a Shinkansen high-speed train derailed on a bridge during the Kumamoto earthquake in 2016. Therefore, it is highly practically significant to investigate the safety performance of trains running on bridges under earthquakes.[2]

To assess the dynamic performance of train-track-bridge coupled system under random multi-point seismic excitations, the dynamic models with different levels of complexity were established. The linear or equivalent linearized wheel-rail contact relations were adopted and the random responses were obtained with the pseudo excitation method (PEM).[3-6] But the wheel-rail forces obtained with these models are quite different from the measured ones, especially when the lateral relative displacements between wheels and rails are large.[7] Therefore, in order to obtain more realistic wheel-rail forces and evaluate the train's running safety performance accurately, the nonlinear wheel-rail contact models considering the effect of practical wheel-rail profiles should be established.

Due to the existence of nonlinear wheel-rail relations, dynamic responses of the vehicle-track-bridge coupled system need to be solved in the time domain.[8] Yang and Wu[9] obtained the equation of motion of a train-bridge coupled system with the dynamic condensation technique, and analysed the effects of four measured seismic excitations on the WDC of a train resting or moving on a bridge. Sogabe et al.[10] developed a nonlinear wheel-rail contact model, and studied the influence of train-running positions and damping ratio of bridge structure on the train's running safety performance under seismic excitations, taking the wheel-rail lateral relative displacement as the index. Ju[11] developed a nonlinear moving wheel element, and discussed the effects of train speed and ground motion on the WDC. Zeng and Dimitrakopoulos[12] determined the normal wheel-rail contact forces and the tangential creep forces according to the linear complementarity method and Shen-Hedrick-Elkins creep theory respectively, and investigated the derailment mechanism of high-speed trains running on bridges under strong earthquakes. Jin et al.[13] presented a nonlinear wheel-rail contact model and investigated the influence of vertical earthquake component on the safety performance of a vehicle moving on a bridge. Montenegro et al.[14] developed a wheel-rail contact element, and analysed the effects of vehicle running speed and seismic intensity on the safety performance of a vehicle moving on a bridge under uniform earthquakes. Xia et al.[15] presented a nonlinear wheel-rail contact model and investigated the effects of train speeds and apparent seismic wave velocities on wheel unloading ratio. Du et al.[16] established a dynamic analysis framework of train-bridge coupled system under non-uniform earthquakes, in which the nonlinear wheel-rail contact geometry relations and wheel-rail separations were considered.

The influence of different factors on the safety performance of trains running on bridges under earthquakes were analysed in the above studies, assuming that the earthquakes occurred at some given moments and ignoring the influence of the earthquake occurrence moments. Li et al.[17] investigated the effects of six earthquake occurrence moments on the dynamic responses of a vehicle travelling on a bridge subjected to uniform seismic excitations, assuming that the vertical displacements at the wheel-bridge contact points were identical. Montenegro[18] analysed the effects of five specific occurrence moments on the safety performance of a vehicle on a bridge under uniform earthquakes. Zeng and Dimitrakopoulos[19] investigated the influence of 11 earthquake occurrence moments on the safety of a train travelling over a bridge under non-uniform seismic excitations. The results of Refs.[17-19] showed that the earthquake occurrence moment had a significant impact on the train's running safety. However, the randomness of the train running positions at the time of the earthquakes was not considered since only several specific deterministic moments were selected.

In this paper, the influence of random multi-point earthquakes on the running safety of a train moving on a long-span bridge is studied from the perspective of dynamic reliability, considering the spatial effects of ground motions, the randomness of seismic excitations and train positions when earthquakes occur. The dynamic model of a train-ballasted track-continuous beam bridge coupled system under the action of spatial multi-point earthquakes is established, as shown in Fig.1. The transition regions between subgrade and bridge are considered. At the support points of track-bridge structure, the propagation direction of vertical earthquake components is along the negative direction of z-axis. The angle between the travelling direction of the seismic waves in the horizontal plane and the x-axis is denoted by γ. The train position when earthquake occurs, measured by the longitudinal position x_{w_1} of wheelset 1, is considered to be a uniformly distributed random variable. The SS method[20,21], which has been widely used for the reliability assessments in engineering areas[22-24], is introduced and combined with the prediction-based iterative method[25] to efficiently assess the safety reliability of a train moving on a bridge under earthquakes. Under different seismic components, train speeds, apparent seismic wave velocities, and seismic intensities, the effects of the earthquake occurrence moments, measured by x_{w_1}, on the safety performance of a train moving through a bridge are analysed. The most unfavourable train position interval can be obtained, providing a guideline for the running safety evaluation of a train moving on a bridge under random seismic excitations.

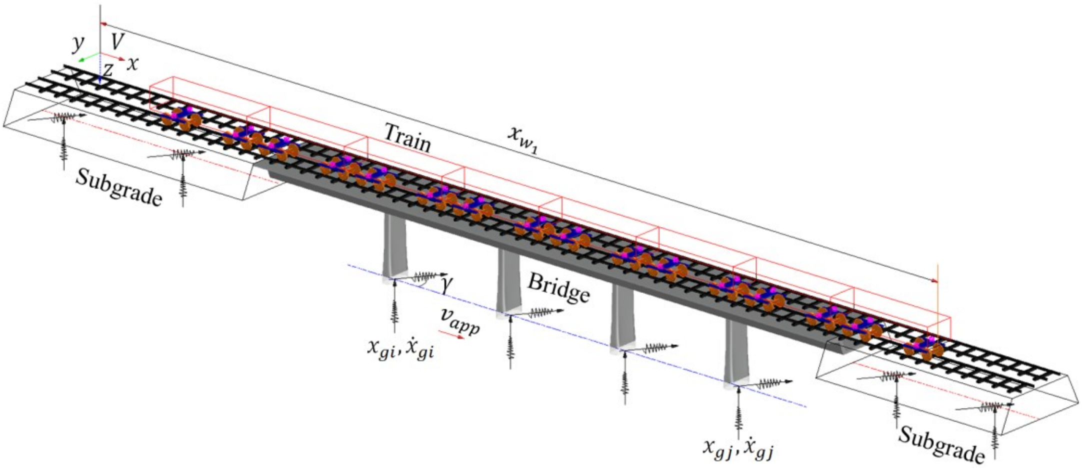

Fig.1. Dynamic model of vehicle-track-bridge system under multi-point seismic excitations

2 Dynamic model of vehicle/track/bridge system under earthquakes

The vehicle/track/bridge coupled system can be divided into two time-invariant subsystems: train subsystem and track-bridge subsystem. The two subsystems are connected at the wheel-rail interface, and the equations of motion of them under seismic excitations are established separately.

2.1 Equation of motion of train subsystem

The seismic excitations act indirectly on the train subsystem through the wheel-rail contact elements. Therefore, the form of the equation of motion of train subsystem will not change whether the seismic excitations are considered or not. A dynamic model of an 8-vehicle CRH2 high-speed train is established in the absolute coordinate system. The interactions between adjacent vehicles are neglected and the parameters of individual vehicles are assumed to be the same.[26-28] Considering the structural characteristics of the vehicle and the damping characteristics of its suspension, a single vehicle is modelled as multiple rigid bodies consisting of one body and two bogies, as shown in Fig.2. Each rigid body has five DOFs other than the longitudinal DOF. The primary and secondary suspensions are modelled as parallel mas-spring-damper elements.

The equation of motion of train subsystem can be written as follows

$$M_v\ddot{X}_v + C_v\dot{X}_v + K_v X_v = F_{vt} \quad (1)$$

where subscript v indicates the train subsystem; $\boldsymbol{X}$, $\dot{\boldsymbol{X}}$ and $\ddot{\boldsymbol{X}}$ denote displacement, velocity and acceleration vectors, respectively; $\boldsymbol{M}$, $\boldsymbol{K}$ and $\boldsymbol{C}$ denote the mass, stiffness and damping matrices, respectively.

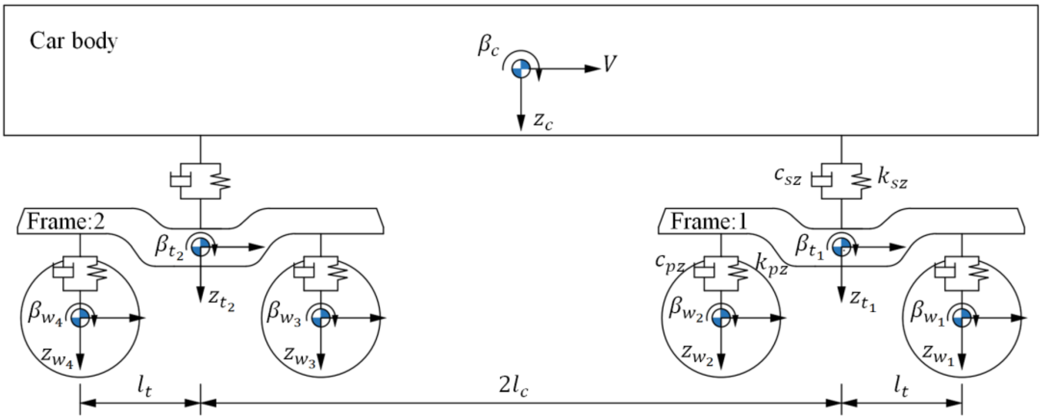

(a) Side view

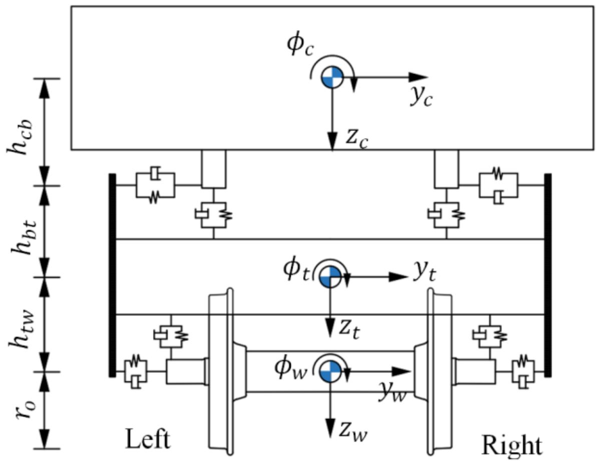

(b) Front view

Fig.2. Dynamic model of railway vehicle subsystem

$$
\begin{cases}
\boldsymbol{X}_v = \{\boldsymbol{x}_{v1}^{\mathrm{T}}, \boldsymbol{x}_{v2}^{\mathrm{T}}, \dots, \boldsymbol{x}_{vN_v}^{\mathrm{T}}\}^{\mathrm{T}} \\
\boldsymbol{M}_v = \mathrm{diag}\left[\boldsymbol{M}_{v1}, \boldsymbol{M}_{v2}, \dots, \boldsymbol{M}_{vN_v}\right] \\
\boldsymbol{K}_v = \mathrm{diag}\left[\boldsymbol{K}_{v1}, \boldsymbol{K}_{v2}, \dots, \boldsymbol{K}_{vN_v}\right] \\
\boldsymbol{C}_v = \mathrm{diag}\left[\boldsymbol{C}_{v1}, \boldsymbol{C}_{v2}, \dots, \boldsymbol{C}_{vN_v}\right]
\end{cases}
\tag{2}
$$

where N_v is the number of vehicles; subscript vi denotes the ith vehicle.

$$
\begin{cases}
\boldsymbol{X}_{vi} = \{\boldsymbol{x}_c^{\mathrm{T}}, \boldsymbol{x}_{t_1}^{\mathrm{T}}, \boldsymbol{x}_{t_2}^{\mathrm{T}}, \boldsymbol{x}_{w_1}^{\mathrm{T}}, \boldsymbol{x}_{w_2}^{\mathrm{T}}, \boldsymbol{x}_{w_3}^{\mathrm{T}}, \boldsymbol{x}_{w_4}^{\mathrm{T}}\}^{\mathrm{T}} \\
\boldsymbol{M}_{vi} = \mathrm{diag}\left[\boldsymbol{M}_c, \boldsymbol{M}_{t_1}, \boldsymbol{M}_{t_2}, \boldsymbol{M}_{w_1}, \boldsymbol{M}_{w_2}, \boldsymbol{M}_{w_3}, \boldsymbol{M}_{w_4}\right] \\
\boldsymbol{K}_{vi} = \begin{bmatrix}
\boldsymbol{K}_{cc} & \boldsymbol{K}_{ct_1} & \boldsymbol{K}_{ct_2} & \boldsymbol{0} & \boldsymbol{0} & \boldsymbol{0} & \boldsymbol{0} \\
\boldsymbol{K}_{t_1c} & \boldsymbol{K}_{t_1t_1} & \boldsymbol{0} & \boldsymbol{K}_{t_1w_1} & \boldsymbol{K}_{t_1w_2} & \boldsymbol{0} & \boldsymbol{0} \\
\boldsymbol{K}_{t_2c} & \boldsymbol{0} & \boldsymbol{K}_{t_2t_2} & \boldsymbol{0} & \boldsymbol{0} & \boldsymbol{K}_{t_2w_3} & \boldsymbol{K}_{t_2w_4} \\
\boldsymbol{0} & \boldsymbol{K}_{w_1t_1} & \boldsymbol{0} & \boldsymbol{K}_{w_1w_1} & \boldsymbol{0} & \boldsymbol{0} & \boldsymbol{0} \\
\boldsymbol{0} & \boldsymbol{K}_{w_2t_1} & \boldsymbol{0} & \boldsymbol{0} & \boldsymbol{K}_{w_2w_2} & \boldsymbol{0} & \boldsymbol{0} \\
\boldsymbol{0} & \boldsymbol{0} & \boldsymbol{K}_{w_3t_2} & \boldsymbol{0} & \boldsymbol{0} & \boldsymbol{K}_{w_3w_3} & \boldsymbol{0} \\
\boldsymbol{0} & \boldsymbol{0} & \boldsymbol{K}_{w_4t_2} & \boldsymbol{0} & \boldsymbol{0} & \boldsymbol{0} & \boldsymbol{K}_{w_4w_4}
\end{bmatrix} \\
\boldsymbol{C}_{vi} = \begin{bmatrix}
\boldsymbol{C}_{cc} & \boldsymbol{C}_{ct_1} & \boldsymbol{C}_{ct_2} & \boldsymbol{0} & \boldsymbol{0} & \boldsymbol{0} & \boldsymbol{0} \\
\boldsymbol{C}_{t_1c} & \boldsymbol{C}_{t_1t_1} & \boldsymbol{0} & \boldsymbol{C}_{t_1w_1} & \boldsymbol{C}_{t_1w_2} & \boldsymbol{0} & \boldsymbol{0} \\
\boldsymbol{C}_{t_2c} & \boldsymbol{0} & \boldsymbol{C}_{t_2t_2} & \boldsymbol{0} & \boldsymbol{0} & \boldsymbol{C}_{t_2w_3} & \boldsymbol{C}_{t_2w_4} \\
\boldsymbol{0} & \boldsymbol{C}_{w_1t_1} & \boldsymbol{0} & \boldsymbol{C}_{w_1w_1} & \boldsymbol{0} & \boldsymbol{0} & \boldsymbol{0} \\
\boldsymbol{0} & \boldsymbol{C}_{w_2t_1} & \boldsymbol{0} & \boldsymbol{0} & \boldsymbol{C}_{w_2w_2} & \boldsymbol{0} & \boldsymbol{0} \\
\boldsymbol{0} & \boldsymbol{0} & \boldsymbol{C}_{w_3t_2} & \boldsymbol{0} & \boldsymbol{0} & \boldsymbol{C}_{w_3w_3} & \boldsymbol{0} \\
\boldsymbol{0} & \boldsymbol{0} & \boldsymbol{C}_{w_4t_2} & \boldsymbol{0} & \boldsymbol{0} & \boldsymbol{0} & \boldsymbol{C}_{w_4w_4}
\end{bmatrix}
\end{cases}
\tag{3}
$$

where subscripts c, t_1, t_2 and $w_i(i = 1\sim4)$ represent the car body, front frame, rear frame and wheelsets 1~4, respectively.

$$
\begin{cases}
\boldsymbol{x}_i = \{y_i, z_i, \phi_i, \beta_i, \psi_i\}^{\mathrm{T}} \\
\boldsymbol{M}_i = \mathrm{diag}[m_i, m_i, I_{ix}, I_{iy}, I_{iz}]
\end{cases}, \quad i = c, t_1, t_2, w_1, w_2, w_3, w_4
\tag{4}
$$

where y and z denote the DOFs in the lateral and vertical directions; ϕ, β and ψ denote the roll, pitch and yaw directions, respectively; m refers to the mass; I_x, I_y and I_z are the moments of inertia about the x, y and z axes, respectively.

The load vector acting on the train system $\boldsymbol{F}_{vt}$ can be written as

$$\boldsymbol{F}_{vt} = \{\boldsymbol{F}_{v1}^{\mathrm{T}}, \boldsymbol{F}_{v2}^{\mathrm{T}}, \dots, \boldsymbol{F}_{vN_v}^{\mathrm{T}}\}^{\mathrm{T}} \tag{5}$$

where

$$\boldsymbol{F}_{vi} = \{\boldsymbol{F}_{c}^{\mathrm{T}}, \boldsymbol{F}_{t_1}^{\mathrm{T}}, \boldsymbol{F}_{t_2}^{\mathrm{T}}, \boldsymbol{F}_{w_1}^{\mathrm{T}}, \boldsymbol{F}_{w_2}^{\mathrm{T}}, \boldsymbol{F}_{w_3}^{\mathrm{T}}, \boldsymbol{F}_{w_4}^{\mathrm{T}}\}^{\mathrm{T}},\ \ i = 1,2,\dots,N_v \tag{6}$$

where $\boldsymbol{F}_c$, $\boldsymbol{F}_{t_1}$, $\boldsymbol{F}_{t_2}$ and $\boldsymbol{F}_{w_i}(i = 1\sim4)$ are the load vectors acting on the car body, front frame, rear frame and wheelsets 1~4, respectively.

$$\begin{cases} \boldsymbol{F}_c = \boldsymbol{F}_{t_1} = \boldsymbol{F}_{t_2} = \boldsymbol{0} \\ \boldsymbol{F}_{w_i} = \begin{bmatrix} F_{iy}^L + F_{iy}^R \\ F_{iz}^L + F_{iz}^R + m_0 g \\ d_0(F_{iz}^R - F_{iz}^L) - r_{w_i}^L F_{iy}^L - r_{w_i}^R F_{iy}^R + I_{w_y}(\dot{\beta}_{wi} - V/r_0)\dot{\psi}_{w_i} \\ r_{w_i}^L F_{ix}^L + r_{w_i}^R F_{ix}^R + \psi_{w_i}(r_{w_i}^R F_{iy}^R + r_{w_i}^L F_{iy}^L) \\ d_0(F_{ix}^L - F_{ix}^R) + d_0\psi_{w_i}(F_{iy}^L - F_{iy}^R) + I_{w_y}\dot{\phi}_{w_i}(\dot{\beta}_{wi} - V/r_0) \end{bmatrix} \end{cases} \tag{7}$$

where F_{ix}^{α}, F_{iy}^{α} and $F_{iz}^{\alpha}(\alpha = L, R)$ are the forces acting on wheels of the ith wheelset in the longitudinal, lateral and vertical direction, respectively; superscripts L and R denote the left and the right sides of the vehicle; $r_{w_i}^{\alpha}$ is the instantaneous wheel rolling radius of the ith wheelset; d_0 is half of the lateral distance between the nominal wheel-rail contact points; ψ_{w_i} is the yaw angle of the ith wheelset; m_0 denotes a quarter of the vehicle mass; g is the gravitational acceleration.

2.2 Equation of motion of track-bridge subsystem

The stiffness and the dynamic characteristics of a bridge under a travelling train are sensitive to the variations of track stiffness.[29] Track structures can effectively attenuate the high-frequency vibration of a vehicle/track/bridge coupled system induced by ground motion, crosswind, out-of-round wheel or rail corrugation.[30] The elastic and damping properties of a track structure have a significant impact on the running safety and ride comfort of trains travelling on bridges.[31] Therefore, the vibrational effects of a track structure need to be taken into account in the study of vehicle-bridge dynamic interaction problems.[32]

Therefore, a dynamic model of track-bridge subsystem under earthquakes is established in the absolute coordinate system, as shown in Fig.3. The effects of the transition regions between the subgrade and the bridge can be considered. The equations of motion of the track and the bridge structures are given respectively, and then coupled together by the track-bridge interaction $\boldsymbol{F}_{tb}$ and $\boldsymbol{F}_{bt}$, as shown by the double arrows in Fig.3, to obtain the equation of motion of the track-bridge subsystem.

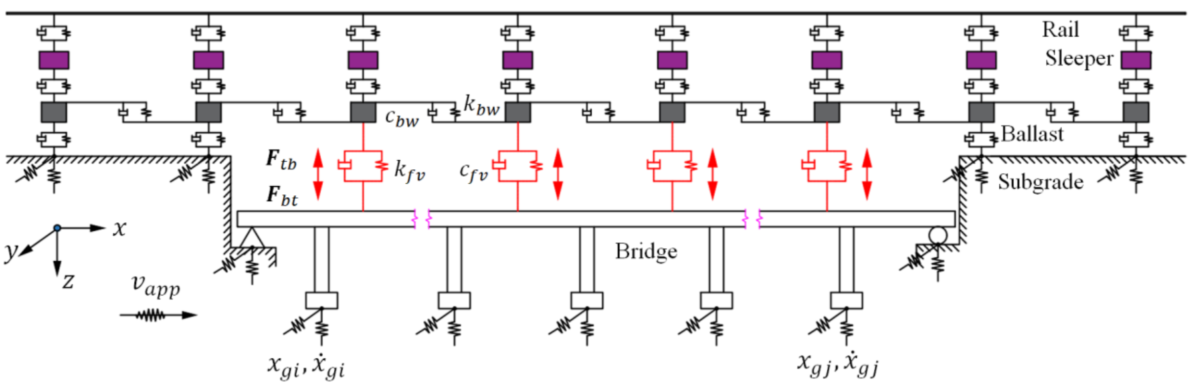

(a) Side view

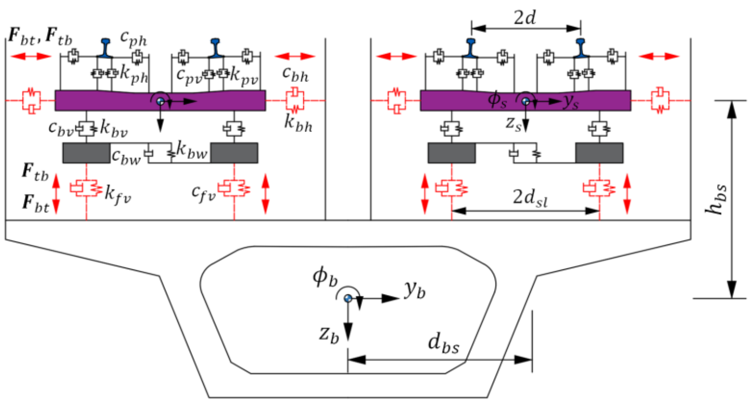

(b) Front view

Fig. 3. Dynamic model of track-bridge subsystem under multi-point seismic excitations

2.2.1 Equation of motion of track structure

The low stiffness of the girder and the large deformation of the bridge deck are unfavourable to the working status of ballastless track. Hence, ballasted tracks are often used for long-span bridges.[33] A dynamic model of three-layer ballasted track[34] is given, consisting of two rails, a number of sleepers and ballast blocks. Each piece of rail is modelled as a simply-supported Euler beam of finite length, considering the bending vibrations in the lateral and vertical directions and the torsional vibration about the rail's longitudinal axis. Each sleeper is modelled as a 3-DOF rigid body in the lateral, vertical and roll directions. The ballast bed consists of a series of ballast blocks. Each ballast block has a vertical DOF only, and the interactions between adjacent ballast blocks are considered. The connections between the components are modelled as parallel spring-damper elements. By rearranging the track matrices according to the DOFs of support and non-support points of track structure, the following equation can be obtained

$$\begin{bmatrix} \boldsymbol{M}_{tt} & \boldsymbol{0} \\ \boldsymbol{0} & \boldsymbol{0} \end{bmatrix} \begin{pmatrix} \ddot{\boldsymbol{X}}_{tt} \\ \ddot{\boldsymbol{X}}_{ss} \end{pmatrix} + \begin{bmatrix} \boldsymbol{C}_{tt} & \boldsymbol{C}_{ts} \\ \boldsymbol{C}_{st} & \boldsymbol{C}_{ss} \end{bmatrix} \begin{pmatrix} \dot{\boldsymbol{X}}_{tt} \\ \dot{\boldsymbol{X}}_{ss} \end{pmatrix} + \begin{bmatrix} \boldsymbol{K}_{tt} & \boldsymbol{K}_{ts} \\ \boldsymbol{K}_{st} & \boldsymbol{K}_{ss} \end{bmatrix} \begin{pmatrix} \boldsymbol{X}_{tt} \\ \boldsymbol{X}_{ss} \end{pmatrix} = \begin{pmatrix} \boldsymbol{F}_{tv} + \boldsymbol{F}_{tb} \\ \boldsymbol{F}_{ts} \end{pmatrix} \tag{8}$$

By expanding the upper part of the Eq. (8), the equation of motion of track structure under earthquakes can be expressed as

$$\boldsymbol{M}_{tt}\ddot{\boldsymbol{X}}_{tt} + \boldsymbol{C}_{tt}\dot{\boldsymbol{X}}_{tt} + \boldsymbol{K}_{tt}\boldsymbol{X}_{tt} = \boldsymbol{F}_{tv} + \boldsymbol{F}_{tb} - \boldsymbol{C}_{ts}\dot{\boldsymbol{X}}_{ss} - \boldsymbol{K}_{ts}\boldsymbol{X}_{ss} \tag{9}$$

where subscript tt denotes the non-support points of subgrade; subscript ss denotes the support points of subgrade; subscripts ts and st denote the coupled part between the support and the non-support points of subgrade; $\boldsymbol{F}_{ts}$ is the load vector of earthquakes acting on the support points of subgrade; $\boldsymbol{F}_{tb}$ denotes the load vector acting on the track structure by the bridge, as shown by the double arrow in Fig.3; $\boldsymbol{F}_{tv}$ is the load vector acting on the track structure by the train, and can be expressed as

$$\boldsymbol{F}_{tv} = \{(\boldsymbol{F}_r^L)^{\mathrm{T}}, (\boldsymbol{F}_r^R)^{\mathrm{T}}, \boldsymbol{F}_s^{\mathrm{T}}, (\boldsymbol{F}_d^L)^{\mathrm{T}}, (\boldsymbol{F}_d^R)^{\mathrm{T}}\}^{\mathrm{T}} \tag{10}$$

where $\boldsymbol{F}_r^L$, $\boldsymbol{F}_r^R$, $\boldsymbol{F}_s$, $\boldsymbol{F}_d^L$ and $\boldsymbol{F}_d^R$ are the load vectors acting on the left rail, the right rail, the sleepers, the left ballast block and the right ballast block, respectively.

$$
\begin{cases}
\boldsymbol{F}_r^L = \left\{ -\sum_{i=1}^{N_w} F_{iy}^L Y_1(x_{w_i}), \dots, -\sum_{i=1}^{N_w} F_{iy}^L Y_{K_r}(x_{w_i}), -\sum_{i=1}^{N_w} F_{iz}^L Z_1(x_{w_i}), \dots, \right. \\
\qquad \left. -\sum_{i=1}^{N_w} F_{iz}^L Z_{K_r}(x_{w_i}), \sum_{i=1}^{N_w} M_{w_i}^L \Phi_1(x_{w_i}), \dots, \sum_{i=1}^{N_w} M_{w_i}^L \Phi_{K_r}(x_{w_i}) \right\}^{\mathrm{T}} \\
\boldsymbol{F}_r^R = \left\{ -\sum_{i=1}^{N_w} F_{iy}^R Y_1(x_{w_i}), \dots, -\sum_{i=1}^{N_w} F_{iy}^R Y_{K_r}(x_{w_i}), -\sum_{i=1}^{N_w} F_{iz}^R Z_1(x_{w_i}), \dots, \right. \\
\qquad \left. -\sum_{i=1}^{N_w} F_{iz}^R Z_{K_r}(x_{w_i}), \sum_{i=1}^{N_w} M_{w_i}^R \Phi_1(x_{w_i}), \dots, \sum_{i=1}^{N_w} M_{w_i}^R \Phi_{K_r}(x_{w_i}) \right\}^{\mathrm{T}} \\
\boldsymbol{F}_s = \boldsymbol{F}_d^L = \boldsymbol{F}_d^R = \boldsymbol{0}
\end{cases}
\tag{11}
$$

where N_w is the number of wheelsets; $Y_k(x)$, $Z_k(x)$ and $\Phi_k(x), (k = 1,2, \dots, K_r)$ are the kth mode shape of the rail in the lateral, vertical and torsional directions, respectively; K_r is the mode truncation order of the rail; x_{w_i} is the longitudinal position of the ith wheelset.

2.2.2 Equation of motion of bridge structure

A 3D finite element model of the bridge is established and the mass matrix $\boldsymbol{M}_b$ and the stiffness matrix $\boldsymbol{K}_b$ are extracted from the ANSYS software. The damping matrix of the bridge $\boldsymbol{C}_b$ takes the proportional damping. By arranging the matrices according to the DOFs of the support and non-support points of the bridge[7], the following equation can be obtained

$$
\begin{bmatrix} \boldsymbol{M}_{bb} & \boldsymbol{0} \\ \boldsymbol{0} & \boldsymbol{M}_{gg} \end{bmatrix} \begin{pmatrix} \ddot{\boldsymbol{X}}_{bb} \\ \ddot{\boldsymbol{X}}_{gg} \end{pmatrix} + \begin{bmatrix} \boldsymbol{C}_{bb} & \boldsymbol{C}_{bg} \\ \boldsymbol{C}_{gb} & \boldsymbol{C}_{gg} \end{bmatrix} \begin{pmatrix} \dot{\boldsymbol{X}}_{bb} \\ \dot{\boldsymbol{X}}_{gg} \end{pmatrix} + \begin{bmatrix} \boldsymbol{K}_{bb} & \boldsymbol{K}_{bg} \\ \boldsymbol{K}_{gb} & \boldsymbol{K}_{gg} \end{bmatrix} \begin{pmatrix} \boldsymbol{X}_{bb} \\ \boldsymbol{X}_{gg} \end{pmatrix} = \begin{pmatrix} \boldsymbol{F}_{bt} \\ \boldsymbol{F}_{bg} \end{pmatrix}
\tag{12}
$$

where $\boldsymbol{M}_{bb}$, $\boldsymbol{K}_{bb}$ and $\boldsymbol{C}_{bb}$ are the mass, stiffness and damping matrices corresponding to the DOFs of non-support points of the bridge, respectively; $\boldsymbol{M}_{gg}$, $\boldsymbol{K}_{gg}$ and $\boldsymbol{C}_{gg}$ are the mass, stiffness and damping matrices corresponding to the DOFs of the bridge support points, respectively; $\boldsymbol{K}_{bg}$ and $\boldsymbol{C}_{bg}$ are the stiffness and damping matrices considering the influence of support points on the non-support support points of the bridge, respectively; $\boldsymbol{K}_{gb}$ and $\boldsymbol{C}_{gb}$ are the stiffness and damping matrices considering the influence of non-support points on the support points of the bridge, respectively; $\boldsymbol{F}_{bt}$ is the load vector acting on the bridge structure by the track, as shown by the double arrow in Fig.3; $\boldsymbol{F}_{bg}$ is the load vector of earthquake acting on the bridge support points.

By expanding the upper part of the Eq. (12), the equation of motion of the bridge structure under earthquakes can be expressed as[9]

$$\boldsymbol{M}_{bb}\ddot{\boldsymbol{X}}_{bb} + \boldsymbol{C}_{bb}\dot{\boldsymbol{X}}_{bb} + \boldsymbol{K}_{bb}\boldsymbol{X}_{bb} = \boldsymbol{F}_{bt} - \boldsymbol{C}_{bg}\dot{\boldsymbol{X}}_{gg} - \boldsymbol{K}_{bg}\boldsymbol{X}_{gg} \tag{13}$$

The proportional damping is assumed and the dynamic responses are solved by the mode superposition method. Let $\boldsymbol{\Phi} = [\boldsymbol{\varphi}_1, \boldsymbol{\varphi}_2, \dots, \boldsymbol{\varphi}_{K_b}]$ be the mass-normalized mode matrix and the influence matrix of pseudo-static displacement $\boldsymbol{R} = -\boldsymbol{K}_{bb}^{-1}\boldsymbol{K}_{bg}$ is introduced. Then, the modal equations of the bridge under seismic excitations can be written as

$$\ddot{\boldsymbol{q}}_b + \widehat{\boldsymbol{C}}_b\dot{\boldsymbol{q}}_b + \widehat{\boldsymbol{\Omega}}_b\boldsymbol{q}_b = \boldsymbol{\Phi}^{\mathrm{T}}\boldsymbol{F}_{bt} + \widehat{\boldsymbol{C}}_b\boldsymbol{\Phi}^{\mathrm{T}}\boldsymbol{M}_{bb}\boldsymbol{R}\dot{\boldsymbol{X}}_{gg} + \widehat{\boldsymbol{\Omega}}_b\boldsymbol{\Phi}^{\mathrm{T}}\boldsymbol{M}_{bb}\boldsymbol{R}\boldsymbol{X}_{gg} \tag{14}$$

where $\boldsymbol{q}_b = \{q_1^b, q_2^b, \dots, q_{K_b}^b\}^{\mathrm{T}}$ is the modal displacement vector of the bridge; The expressions of $\widehat{\boldsymbol{\Omega}}_b$ and $\widehat{\boldsymbol{C}}_b$ can be given as follows

$$\begin{cases} \widehat{\boldsymbol{\Omega}}_b = \boldsymbol{\Phi}^{\mathrm{T}}\boldsymbol{K}_{bb}\boldsymbol{\Phi} = \mathrm{diag}\left[\omega_1^2, \omega_2^2, \dots, \omega_{K_b}^2\right] \\ \widehat{\boldsymbol{C}}_b = \boldsymbol{\Phi}^{\mathrm{T}}\boldsymbol{C}_{bb}\boldsymbol{\Phi} = \mathrm{diag}[2\xi_1\omega_1, 2\xi_2\omega_2, \dots, 2\xi_{K_b}\omega_{K_b}] \end{cases} \tag{15}$$

where ξ_i and ω_i are the damping ratio and natural frequency of the ith mode, respectively;

K_b is the number of modes used for the bridge structure.

2.2.3 Track-bridge dynamic interaction

Different forms of track structures on bridges lead to different transmission paths of the track-bridge interaction forces $\boldsymbol{F}_{tb}$ and $\boldsymbol{F}_{bt}$. For the ballasted track, the bridge structure interacts with the sleepers in the lateral direction, and with the ballast blocks in the vertical direction, as shown by the double arrow in Fig.3.

The equivalent force and moment of the track structure acting on the bridge at the position of the jth sleeper can be expressed as

$$\begin{cases} F_{bshj} = F_{bshj}^{L} + F_{bshj}^{R} \\ F_{bdvj} = F_{bdvj}^{L} + F_{bdvj}^{R} \\ M_{bt} = F_{bshj} h_{bs} + F_{bdvj}^{L}(d_{bs} - d) + F_{bdvj}^{R}(d_{bs} + d) \end{cases} \tag{16}$$

where $F_{bshj}^{\alpha}, (\alpha = L, R)$ are the lateral forces acting on the bridge at the left and right ends of the jth sleeper; $F_{bdvj}^{\alpha}, (\alpha = L, R)$ are the vertical forces acting on the bridge by the left and right ballast blocks at the position of the jth sleeper, respectively.

$$\begin{cases} F_{bshj}^{L} = F_{bshj}^{R} = k_{bh}\left(y_{s_j} - y_{b_j} - h_{bs}\phi_{b_j}\right) + c_{bh}\left(\dot{y}_{s_j} - \dot{y}_{b_j} - h_{bs}\dot{\phi}_{b_j}\right) \\ F_{bdvj}^{L} = k_{fv}\left(z_{d_j}^{L} - z_{b_j} - (d_{bs} - d_{sl})\phi_{b_j}\right) + c_{fv}\left(\dot{z}_{d_j}^{L} - \dot{z}_{b_j} - (d_{bs} - d_{sl})\dot{\phi}_{b_j}\right) \\ F_{bdvj}^{R} = k_{fv}\left(z_{d_j}^{R} - z_{b_j} - (d_{bs} + d_{sl})\phi_{b_j}\right) + c_{fv}\left(\dot{z}_{d_j}^{R} - \dot{z}_{b_j} - (d_{bs} + d_{sl})\dot{\phi}_{b_j}\right) \end{cases} \tag{17}$$

where k_{bh} and c_{bh} are the lateral stiffness and damping coefficients between the sleeper and the bridge, respectively; k_{fv} and c_{fv} are the vertical stiffness and damping coefficient between the ballast blocks and the bridge, respectively; h_{bs} is the vertical distance from the centroid of the bridge girder to the centre of mass (COM) of the sleeper; d_{sl} is the lateral distance between the left and the right ballast blocks; d_{bs} is the lateral distance from the centroid of the bridge girder to the COM of the sleeper; y_{b_j}, z_{b_j} and ϕ_{b_j} are the lateral, vertical displacements and the torsional angular displacement of the bridge girder at the position of the jth sleeper, respectively; y_{s_j}, z_{s_j} and ϕ_{s_j} are the lateral, vertical displacements and roll angle of the jth sleeper, respectively; $z_{d_j}^L$ and $z_{d_j}^R$ are the vertical displacements of the left and the right ballast blocks, respectively.

The loads acting on the nodes of the bridge FE model can be obtained by decomposition of equivalent force and moment. Then, the load vector $\boldsymbol{F}_{bt}$ acting on the bridge by the track can be obtained by assembling the nodal loads according to the nodal DOFs of the bridge. The load vector $\boldsymbol{F}_{tb}$ acting on the track by the bridge can be obtained by assembling the lateral force $F_{sbhj}^{\alpha} = -F_{bshj}^{\alpha}$ and the vertical force $F_{dbvj}^{\alpha} = -F_{bdvj}^{\alpha}$ according to the DOFs of the track structure. By substituting $\boldsymbol{F}_{tb}$ into Eq. (9) and $\boldsymbol{F}_{bt}$ into Eq. (14), the equation of motion of the track-bridge subsystem under earthquakes can be written as

$$\begin{bmatrix} \boldsymbol{M}_{tt} & \boldsymbol{0} \\ \boldsymbol{0} & \boldsymbol{I} \end{bmatrix} \begin{pmatrix} \ddot{\boldsymbol{X}}_{tt} \\ \ddot{\boldsymbol{q}}_b \end{pmatrix} + \begin{bmatrix} \boldsymbol{C}_{tt} & \boldsymbol{C}_{tb} \\ \boldsymbol{C}_{bt} & \widehat{\boldsymbol{C}}_b \end{bmatrix} \begin{pmatrix} \dot{\boldsymbol{X}}_{tt} \\ \dot{\boldsymbol{q}}_b \end{pmatrix} + \begin{bmatrix} \boldsymbol{K}_{tt} & \boldsymbol{K}_{tb} \\ \boldsymbol{K}_{bt} & \widehat{\boldsymbol{\Omega}}_b \end{bmatrix} \begin{pmatrix} \boldsymbol{X}_{tt} \\ \boldsymbol{q}_b \end{pmatrix} = \begin{pmatrix} \boldsymbol{F}_{tv} - \left(\boldsymbol{C}_{ts}\dot{\boldsymbol{X}}_{ss} + \boldsymbol{K}_{ts}\boldsymbol{X}_{ss}\right) \\ \widehat{\boldsymbol{C}}_b\boldsymbol{\Phi}^{\mathrm{T}}\boldsymbol{M}_{bb}\boldsymbol{R}\dot{\boldsymbol{X}}_{gg} + \widehat{\boldsymbol{\Omega}}_b\boldsymbol{\Phi}^{\mathrm{T}}\boldsymbol{M}_{bb}\boldsymbol{R}\boldsymbol{X}_{gg} \end{pmatrix} \tag{18}$$

2.3 Nonlinear wheel-rail contact model

The LMA wheel profile and the CHN60 rail profile are adopted respectively. The contact positions, contact angles, vertical compression and creepage between wheels and rails are determined using the “new wheel-rail spatial contact model” proposed by Chen and Zhai.[35] The instantaneous wheel-rail detachment can be considered and the iterative solution of wheelset roll angle can be avoided. The wheel-rail spatial contact position is shown in Fig.4.

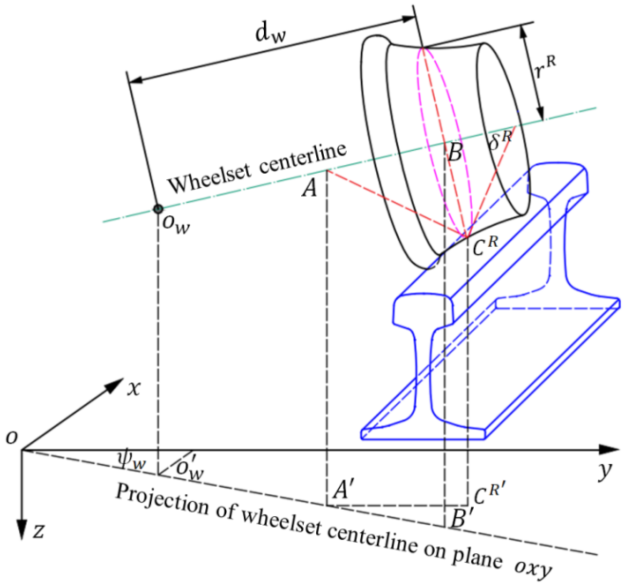

Fig.4. Schematic diagram of wheel-rail spatial contact position

Firstly, at a certain moment, the spatial curve consisting of a series of possible contact points C^R on the wheel profile, named "contact locus", can be obtained according to the trace method.[36]

$$\begin{cases} x_c = -\cos\phi_w \sin\psi_w (d_w + r^R \tan\delta^R) \\ y_c = d_w(\cos\phi_w \cos\psi_w) - \dfrac{r^R(\cos^3\phi_w \sin^2\psi_w \cos\psi_w \tan\delta^R + H\sin\phi_w)}{1-(\cos\phi_w \sin\psi_w)^2} + y_w \\ z_c = d_w \sin\phi_w - \dfrac{r^R(\cos^2\phi_w \sin\phi_w \sin^2\psi_w \tan\delta^R - H\cos\phi_w \cos\psi_w)}{1-(\cos\phi_w \sin\psi_w)^2} \end{cases} \tag{19}$$

where y_w, ϕ_w and ψ_w are the lateral displacement, roll and yaw angles of the wheelset, respectively; r^R and δ^R denote the instant rolling radius and contact angle of the right wheel, respectively; $H = \sqrt{1-(\cos\phi_w \sin\psi_w)^2(1+\tan^2\delta^R)}$; d_w is the lateral coordinate of the centre of the wheel rolling circle in the wheelset coordinate system.

Then the minimum vertical distance between the contact locus and the rail profile is found, and the position of minimum vertical distance is considered as the wheel-rail contact point. The parameters, such as the curvature of the profiles, the contact angles and the normal compression between wheels and rails at the contact positions, can be obtained. Finally, the normal wheel-rail forces are obtained according to the nonlinear Hertzian theory.[34]

$$N_{iz_c}^{\alpha}(t) = \begin{cases} \left[\delta Z_{iz_c}^{\alpha}/G\right]^{3/2} & \delta Z_{iz_c}^{\alpha} > 0 \\ 0 & \delta Z_{iz_c}^{\alpha} \le 0 \end{cases} \tag{20}$$

where $G = 3.86 r_0^{-0.115} \times 10^{-8} (\mathrm{m/N^{2/3}})$ is the wheel-rail contact constant;[34] r_0 is the wheel nominal radius; $\delta Z_{iz_c}^{\alpha}$ is the normal displacement at the wheel-rail contact point, and $\delta Z_{iz_c}^{\alpha} \le 0$ means that the wheel lifts off from the rail. The tangential wheel-rail creep forces are calculated by the FASTSIM algorithm, considering the influence of the change rate of track irregularities.[37]

2.4 Generation of non-stationary multi-point earthquake samples

Since the nonlinear wheel-rail relations are considered in the dynamic model, the dynamic responses of the vehicle/track (bridge) coupled system need to be obtained in the time domain. The seismic excitations at the track-bridge support points are different due to the spatial effects, which can be described by the cross-spectral density matrix of acceleration at each support point.[38] The samples of ground motions can be generated according to the time-frequency transform method. The trigonometric series method has been widely used in the generation of time-domain samples of ground motions, but the randomness of samples comes from the random phases uniformly distributed over the interval $[0,2\pi]$. Moreover, the influence of phase change on the generated samples is global, which reduces the efficiency and the accuracy of the SS method.[39] In order to overcome this problem, the ARMA model[40] is applied to generate the samples of ground motions. The randomness of samples is derived from a series of independent and identically distributed random variables and the effects of random variables on the samples are local. Therefore, the ARMA model can be well applied to the SS method.[39]

Based on the ARMA model, the method for generating the time-history samples of multi-point non-stationary seismic acceleration is given as follows:

Step 1: Determining the PSD function of ground acceleration according to the site conditions. The Clough-Penzien acceleration PSD[41] is used.

$$S(\omega) = \frac{1 + 4\xi_g^2(\omega/\omega_g)^2}{\left[1 - (\omega/\omega_g)^2\right]^2 + 4\xi_g^2(\omega/\omega_g)^2} \cdot \frac{\omega^4}{(\omega^2 - \omega_f^2)^2 + 4\omega^2\omega_f^2\xi_f^2} S \tag{21}$$

where subscripts g and f denote the site and the filter, respectively; ω denotes the angular frequency in rad/s; ξ denotes the modal damping ratio; S indicates the spectrum intensity.

Step 2: Choosing the adopted coherence function as follows

$$\gamma(\omega, d) = \exp\left(-\frac{\mathrm{i}\omega d_{ij}^S}{v_{app}}\right)\exp\left(-\zeta\frac{\omega d_{ij}}{2\pi v_{app}}\right) \tag{22}$$

where $\exp(-\mathrm{i}\omega d_{ij}^L/v_{app})$ and $\exp(-\alpha\omega d_{ij}/2\pi v_{app})$ reflect the effects of wave propagation and incoherence, respectively; d_{ij} is the horizontal distance between support points i and j; d_{ij}^S is the projection of d_{ij} in the travelling direction of the seismic wave;

v_{app} is the apparent seismic wave velocity; ζ is the incoherence factor, and ζ =0.125 is recommended.[42]

Step 3: Selecting the uniform modulation function. The uniform modulation function adopted[3] in this paper is written as

$$G(\omega,t)=G(t)=\begin{cases}(t/t_b)^2 & 0\le t<t_b\\ 1 & t_b\le t<t_c\\ \exp(-c(t-t_c)) & t\ge t_c\end{cases} \tag{23}$$

where c is the seismic attenuation coefficient; t_b and t_c are the beginning and ending moments of the seismic stationary stage, respectively.

Step 4: Calculating the cross-PSD function matrix of seismic acceleration of M support points at t_k moment

$$\boldsymbol{S}(\omega_h,t_k)=\begin{bmatrix}S_{11} & S_{12} & \cdots & S_{1M}\\ S_{21} & S_{22} & \cdots & S_{2M}\\ \vdots & \vdots & \ddots & \vdots\\ S_{M1} & S_{M2} & \cdots & S_{MM}\end{bmatrix} \tag{24}$$

where

$$S_{ij}=\begin{cases}|G_i(\omega_h,t_k)|^2 S_i(\omega_h) & (i=j)\\ G_i(\omega_h,t_k)G_j(\omega_h,t_k)\sqrt{S_i(\omega_h)S_j(\omega_h)}\gamma_{ij}(\omega_h,t_k) & (i\ne j)\end{cases} \tag{25}$$

where S_i and S_j denote the auto-PSDs of the support points of i and j respectively, and reflect the local site effect; $\omega_h=h\omega_u/N_\omega,(h=1,2,\dots,N_\omega)$; N_ω is the number of discrete frequency points, ω_u is the upper limit of the cut-off frequency.

Step5: According to the ARMA model, the time-history samples of seismic acceleration $\boldsymbol{U}(t)$ of M support points can be expressed as

$$\boldsymbol{U}(t)=\sum_{i=1}^{p}\boldsymbol{A}_i\boldsymbol{U}(t-i\Delta t)+\sum_{j=0}^{q}\boldsymbol{B}_j\boldsymbol{W}(t-j\Delta t) \tag{26}$$

where p and q denote the orders of AR and MA models, respectively; $\boldsymbol{A}_i$ and $\boldsymbol{B}_j$ are the autoregressive coefficient matrix and the moving average coefficient matrix, respectively; $\boldsymbol{W}(t)$ denotes the white noise random vector composed of the independent and identically distributed random variables; Δt is the time interval of time history samples. It can be seen from Eq. (25) that the key to generating the time-history samples is to determine coefficient $\boldsymbol{A}_i$ and $\boldsymbol{B}_j$ according to matrix $\boldsymbol{S}(\omega_h,t_k)$. The detailed method can be found in Ref.[42].

The solution accuracy is higher for the FE model under the seismic acceleration input mode, while better calculation accuracy can be obtained for the modal model under the displacement-velocity input mode.[22] It can be seen from Eq. (18) that the time-history samples of seismic velocity and displacement are needed. Therefore, the seismic acceleration data obtained by the above steps needs to be integrated to obtain the time-history samples of seismic velocity and displacement. However, the integral correction methods, such as the least-squares fitting method[43], are required to eliminate the baseline offset caused by numerical integration. The ground motions directly act on the subgrade/bridge support points in the form of displacement and velocity,[9] and indirectly act on the train subsystem through the wheel-rail contact relation.

The integral correction method of eliminating the baseline offset is given as follows[43]. It is assumed that the baseline form of seismic displacement time series is

$$\tilde{u}_g(t) = a_1t^4 + a_2t^3 + a_3t^2 + a_4t \tag{27}$$

Then the baseline form of seismic velocity and acceleration can be expressed as

$$\begin{cases} \dot{\tilde{u}}_g(t) = 4a_1t^3 + 3a_2t^2 + 2a_3t + a_4 \\ \ddot{\tilde{u}}_g(t) = 12a_1t^2 + 6a_2t + 2a_3 \end{cases} \tag{28}$$

where a_1, a_2, a_3 and a_4 are the four constants to be determined. Noting in the common practice in seismic analysis, the initial velocity and displacement of the system are assumed to be zero, then the coefficient a_4 can be determined. The remaining three coefficients are determined here by minimizing mean square value of the acceleration as

$$\mathrm{Min}\left\{\sum_{i=1}^{N}[(\ddot{u}_{gi} - \ddot{\tilde{u}}_{gi})^2]\right\} = \mathrm{Min}\left\{\sum_{i=1}^{N}[(\ddot{u}_{gi} - (12a_1t_i^2 + 6a_2t_i + 2a_3))^2]\right\} \tag{29}$$

where $\ddot{u}_{gi}$ is the ground acceleration time series that is either recorded or synthesized.

The acceleration is then corrected by subtracting $\ddot{\tilde{u}}_g(t)$ from $\ddot{u}_g(t)$ when the baseline of the acceleration is completely determined. A windowed filter is designed for further processing the baseline-corrected acceleration data in the frequency domain. The filter can be expressed as

$$\beta(T) = \begin{cases} 1 & 0 \le T \le T_0 \\ e^{-(T-T_0)/a} & T > T_0 \end{cases} \tag{30}$$

where a and T_0 are the parameters that can be determined by using two key points A and B, which are selected based on the characteristics of the Fourier spectra of the displacement time series derived by integrating the uncorrected and baseline-corrected acceleration data.

After obtaining the corrected seismic acceleration, the velocity and the displacement are derived by single or doubly integrating the corrected acceleration.

2.5 Solution of dynamic responses

The dynamic responses of the train/track/bridge coupled system can be determined by the prediction-based iterative solution method, in which the regeneration of coefficient matrices of the whole system at each time step can be avoided. Hence, the solution efficiency of the dynamic responses of trains passing through long-span bridges is enhanced[7]. The prediction iterative method proposed by the authors[25] is used to determine the dynamic responses of the train/track/bridge coupled system, so as to further improve the calculation efficiency. The main difference between the prediction iterative method and the conventional iterative method lies in the different ways of obtaining the initial value at each time step: the prediction iterative method takes the wheel-rail force calculated by the Weighted Least-Squares Error (WLSE) predictor[44], while the conventional iterative method takes the last converged value of the previous time step.

Taking the wheel-rail vertical force F_{iz}^{α} as an example, according to the WLSE prediction method, the predicted force at time t_n is given as follows

$$\hat{F}_{iz,n}^{\alpha} = \sum_{\vartheta=1}^{P} a_{n-\vartheta}^{\alpha} F_{iz,n-\vartheta}^{\alpha} = (\boldsymbol{a}_n^{\alpha})^{\mathrm{T}} \overline{\boldsymbol{F}}_n^{\alpha} \tag{31}$$

where $\boldsymbol{a}_n^{\alpha} = \{a_{n-1}^{\alpha}, a_{n-2}^{\alpha}, \dots, a_{n-P}^{\alpha}\}^{\mathrm{T}}$ is a vector of prediction coefficient $a_{n-\vartheta}^{\alpha}$; P is the prediction order; $\overline{\boldsymbol{F}}_n^{\alpha} = \{F_{iz,n-1}^{\alpha}, F_{iz,n-2}^{\alpha}, \dots, F_{iz,n-P}^{\alpha}\}^{\mathrm{T}}$ is the P known forces before time t_n.

The method for determining the prediction coefficient vector $\boldsymbol{a}_n^\alpha$ is as follows:

Step 1: Setting the predicted force at time t_1: $\hat{F}_{iz,1}^\alpha = F_{iz,1}^\alpha$, where $F_{iz,1}^\alpha$ is calculated by the conventional iterative method.

Step 2: Calculating the force $\hat{F}_{iz,n}^\alpha$ at time t_n for $2 \le n \le N_c$

$$\hat{F}_{iz,n}^\alpha = (\boldsymbol{a}_n^\alpha)^{\mathrm{T}} \overline{\boldsymbol{F}}_n^\alpha \tag{32}$$

where $\boldsymbol{a}_2^\alpha = \{1,0,\dots,0\}^{\mathrm{T}}$, $\overline{\boldsymbol{F}}_n^\alpha = \{F_{iz,n-1}^\alpha, F_{iz,n-2}^\alpha, \dots, F_{iz,n-M}^\alpha\}^{\mathrm{T}}$, in which the forces with the subscript less than or equal to zero are set to zero.

Step 3: Updating the prediction coefficient vector as

$$\boldsymbol{a}_{n+1}^\alpha = \boldsymbol{a}_n^\alpha + \frac{\boldsymbol{B}_n^\alpha \overline{\boldsymbol{F}}_n^\alpha}{\xi + (\overline{\boldsymbol{F}}_n^\alpha)^{\mathrm{T}} \boldsymbol{B}_n^\alpha \overline{\boldsymbol{F}}_n^\alpha} [F_{iz,n}^\alpha - \hat{F}_{iz,n}^\alpha] \tag{33}$$

where $\boldsymbol{B}_2^\alpha = \boldsymbol{I}$ (identity matrix of order M). ξ is sometimes also referred to as the forgetting factor and $\xi = 0.99$ is usually used.

Step 4: Renewing matrix $\boldsymbol{B}$ as

$$\boldsymbol{B}_{n+1}^\alpha = \frac{1}{\xi}\left\{\boldsymbol{B}_n^\alpha - \frac{\boldsymbol{B}_n^\alpha \overline{\boldsymbol{F}}_n^\alpha (\overline{\boldsymbol{F}}_n^\alpha)^{\mathrm{T}} \boldsymbol{B}_n^\alpha}{\xi + (\overline{\boldsymbol{F}}_n^\alpha)^{\mathrm{T}} \boldsymbol{B}_n^\alpha \overline{\boldsymbol{F}}_n^\alpha}\right\} \tag{34}$$

Step 5: Returning to Step 2 for the next time step until the calculation is finished.

The predicted wheel-rail forces are corrected by the nonlinear wheel-rail contact model, and the iteration within a time step continues until the accuracy requirement is satisfied. The convergence condition is that the relative errors of the lateral and vertical wheel-rail forces in the two adjacent iteration steps are less than the limit values. Then the wheel-rail forces satisfying the accuracy are substituted into the equations of motion, and the dynamic responses are obtained with the new simple explicit integration method proposed by Zhai.[45] If the error between the predicted and corrected forces meets the convergence criterion, the number of iterations can be significantly reduced. The detailed iterative solution process can be found in Ref.[25].

3 Train running safety reliability evaluation by SS

Although the Monte Carlo simulation (MCS) method can be used for solving the failure probability of the train/track/bridge coupled system, a large amount of samples is needed, especially when the failure probability is small. Thus, the SS method proposed by Au et al. [20,21] is introduced into the train/track/bridge coupled system to evaluate the running safety reliability of a train moving on a long-span bridge under earthquakes.

The solution strategy of the SS method is to introduce l incremental intermediate limit values $0 < b_1 < b_2 < \cdots < b_l = b$ to construct the intermediate failure events $F_1 \supset F_2 \supset \cdots \supset F_l = F$ with nested relations. b is the limit value of the response index. l is the number of levels of the SS method. According to the nesting characteristics, the failure probability P_F can be expressed as the product of $P(F_1)$ and a series of conditional probabilities $P(F_j|F_{j-1})$

$$P_F = P(F) = P(F_1)\prod_{j=2}^{l} P(F_j|F_{j-1}) = \prod_{j=1}^{l} P_j \tag{35}$$

where $P_1 = P(F_1)$, $P_j = P(F_j|F_{j-1}), (j = 2, \cdots, l)$.

The train position at the time of the earthquake is considered a random variable, and the seismic excitation is considered a random field. P_1 is calculated from the random samples generated based on the assumed probability density function (PDF) $q(\boldsymbol{\theta})$. $P_j, (j = 2,3,\cdots,l)$ can be calculated from the samples generated according to the conditional PDF $q(\boldsymbol{\theta}|F_j) = q(\boldsymbol{\theta})I_{F_j}(\boldsymbol{\theta})/P(F_j)$. The Modified Metropolis Algorithm (MMA) algorithm[23] is used to obtain samples that satisfy the given conditional PSD $q(\boldsymbol{\theta}|F_j)$, which is a complex function that can't even be explicitly expressed. After obtaining the random samples, $P_j, (j = 1,2,\cdots,l)$ can be calculated as follows

$$P_j = \frac{1}{N_s}\sum_{h=1}^{N_s} I_{F_j}\left(\boldsymbol{\theta}_h^{(i)}\right), (j = 1,2,\cdots,l) \tag{36}$$

where $\boldsymbol{\theta}_h^{(1)}$ denotes the samples generated from the PSD $q(\boldsymbol{\theta})$; $\boldsymbol{\theta}_h^{(j)}, (j = 2,3,\cdots,l)$ denotes the samples generated from the conditional PDF $q(\boldsymbol{\theta}|F_j)$; N_s is the number of samples at each level.

By substituting Eq. (36) into Eq. (35), P_F can be expressed as

$$P_F = p_0^{l-1}\frac{1}{N_s}\sum_{h=1}^{N_s} I_{F_l}\left(\boldsymbol{\theta}_h^{(l)}\right) \tag{37}$$

where p_0 denotes the level failure probability, and p_0 =0.1 is recommended.[24]

According to the SS method, a low failure probability can be expressed as the product of a series of high conditional probabilities, and the samples corresponding to the conditional PDF are generated by the MMA method. Hence the number of samples needed for the reliability evaluation is reduced and the calculation efficiency is effectively improved.

4 Numerical examples

The dynamic analysis of the train/track/bridge coupled system under earthquakes mainly focuses on the influence of ground motions on the train running safety.[7] Both the track and the bridge structure are assumed to deform elastically without damage. The train running safety performance can be characterised by the WDC, which is defined as the ratio of the lateral force to the vertical force at the same position. The limit value of the WDC is 0.8.[46] The parameters of the vehicle and the track subsystem are detailed in Ref.[25].

A 12-span bridge with length L_b of 720m is adopted, as shown in Fig. 5. A 3D finite element model of the bridge is established in ANSYS and the 3D beam element (BEAM188) of 2 m is used. The cross-sectional properties of the girder and the pier are given in Table 1. Density ρ =2500kg/m^3 and the Poisson's ratio $\nu = 0.3$. The natural frequencies of 12-span continuous bridge are given in Table 2.

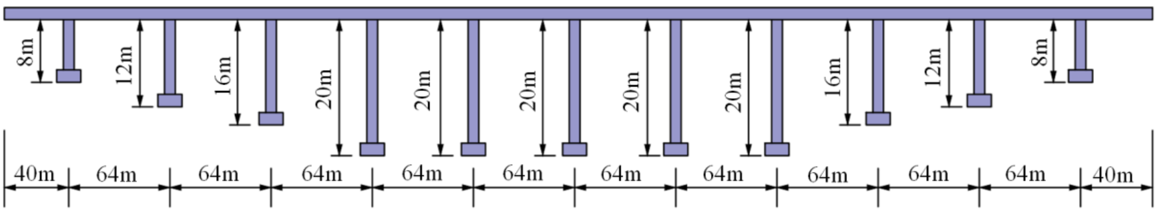

Fig. 5. Schematic diagram of 12-span continuous bridge

Table 1 Cross-section properties of the girder and the pier

Parameter	Girder	Pier	Unit

Cross-sectional area	12.83	6.2	m^2
Torsional moment of inertia	51.9	10.17	m^4
Bending moment of inertia around the y axis	134	28.7	m^4
Bending moment of inertia around the z axis	19.2	2.4	m^4
Elastic modulus	2.5×10^{10}	4×10^{10}	N/m^2

Table 2 Natural frequencies of 12-span continuous bridge

Mode	Frequency (Hz)									
1-10	1.884	1.956	1.993	2.034	2.062	2.081	2.301	2.301	2.646	2.710
11-20	2.711	4.145	4.310	4.391	4.428	4.663	4.744	4.752	5.022	5.177
91-100	28.231	28.588	28.759	29.381	29.979	30.394	30.552	31.356	31.703	31.895

The modal superposition method is used to obtain the dynamic responses of the bridge structure, and the first 300 modes are selected. The proportional damping is assumed and the damping ratio of each mode takes 0.02. The number of samples at each level of the SS method is 1000, and the time step $\Delta t = 10^{-4}$s.

Assuming that the train runs from the left to the right along the track, the seismic wave travels along the train running direction, and the duration of the earthquake is the same as the train running time. The initial position of the train is shown in Fig.6. The track irregularities measured on Beijing-Tianjin railway line are employed, and the randomness of track irregularities is ignored. Taking the maximum WDC of the first vehicle as the index, the running safety reliability of the train moving on the bridge under earthquakes is evaluated. The effects of the earthquake occurrence moment on the safety performance of the train moving on the bridge are analysed under different seismic components, train speeds, apparent seismic wave velocities and seismic intensities. The earthquake occurrence moment is represented by the longitudinal position of the first wheel x_{w_1}, as shown in Fig.6.

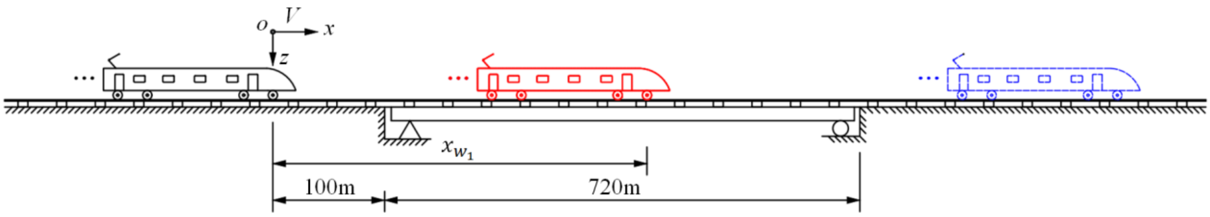

Fig. 6. Schematic diagram of the initial position of the train

4.1 Different seismic components

There are two main components of seismic excitations: vertical and horizontal.[7] The vertical seismic component is imposed in the negative direction of z axis. The propagation direction of the horizontal seismic component is at angle γ with respect to the x axis, as shown in Fig.1. The effects of seismic components on the WDC are studied in three cases: only impose the lateral seismic component ($\gamma = 90^{\circ}$), only impose the vertical seismic component and impose the above two components simultaneously. The train speed V is 200km/h and the apparent seismic wave velocity v_{app} =1000m/s. The correlation between the horizontal and the vertical seismic components is neglected. The PSD parameters of the earthquake acceleration are selected as follows[3]

$$S_v = 0.218 S_h; \quad \omega_{gv} = 1.58\omega_{gh}; \quad \xi_{gv} = \xi_{gh}; \quad \xi_{fh} = \xi_{gh}$$
$$\omega_{fh} = 0.1\omega_{gh} \sim 0.2\omega_{gh}; \quad \xi_{fv} = \xi_{gv}; \quad \omega_{fv} = 0.1\omega_{gv} \sim 0.2\omega_{gv} \tag{38}$$

where subscripts v and h represent the horizontal and vertical seismic components, respectively; $S_h = 7.0 \times 10^{-4}$m^2/s^3, ω_{gh} =17.95rad/s, ξ_{gh} =0.72. The parameters of the uniform modulation function are taken as: c =0.25, t_b =1.2s and t_c =9s.

Under the combined action of the lateral and vertical seismic components, the failure probability distribution (FPD) curves of the WDC obtained by the SS method with 4 levels (3700 samples) and the MCS with 10,000 samples are shown in Fig.7. It can be seen that the FPD curves obtained by the two methods agree well when the failure probability of WDC is greater than 8.75×10^{-4}. However, the difference between the two methods increases when the failure probability of WDC is less than 8.75×10^{-4} due to the uncertainty of MCS. The results show that the SS method can be effectively used for the safety reliability evaluation of the trains moving on the bridges.

According to the SS method, the FPD curves of WDC under different seismic components are also given in Fig.7. It shows that the FPD curve under the lateral seismic component is close to that under the combined action of the lateral and vertical seismic components, while the FPD curve under the vertical seismic component is quite different. The failure probability of the WDC is smaller when only the vertical seismic component is considered. It shows that the lateral seismic component has a significant influence on the WDC, comparing with the vertical seismic component. This is because the wheel-rail forces vary greatly, as shown in Fig.8 and Fig.9, due to the large relative displacements between wheels and rails under lateral seismic component. This conclusion obtained agrees well with the Refs.[11,47], verifying the method used in this paper.

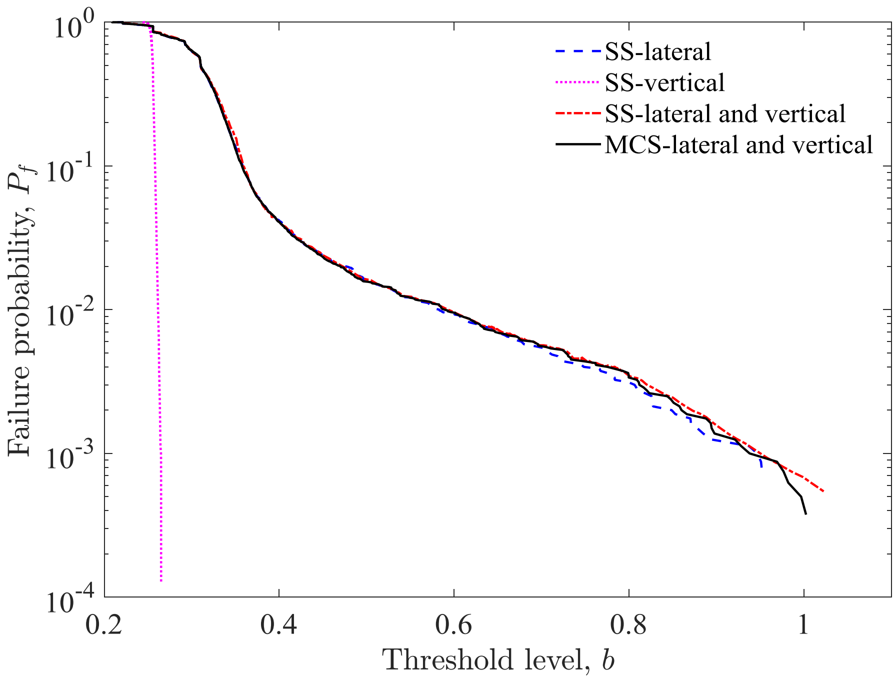

Fig. 7. FPD curves of the WDC under different seismic components

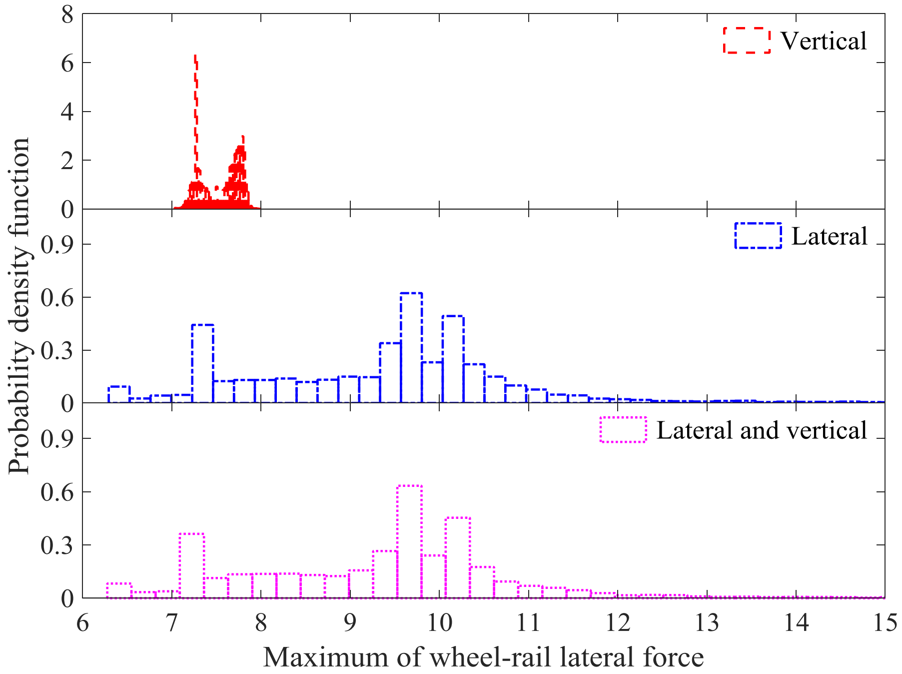

Fig. 8. Distribution of maximum wheel-rail lateral force under different seismic components

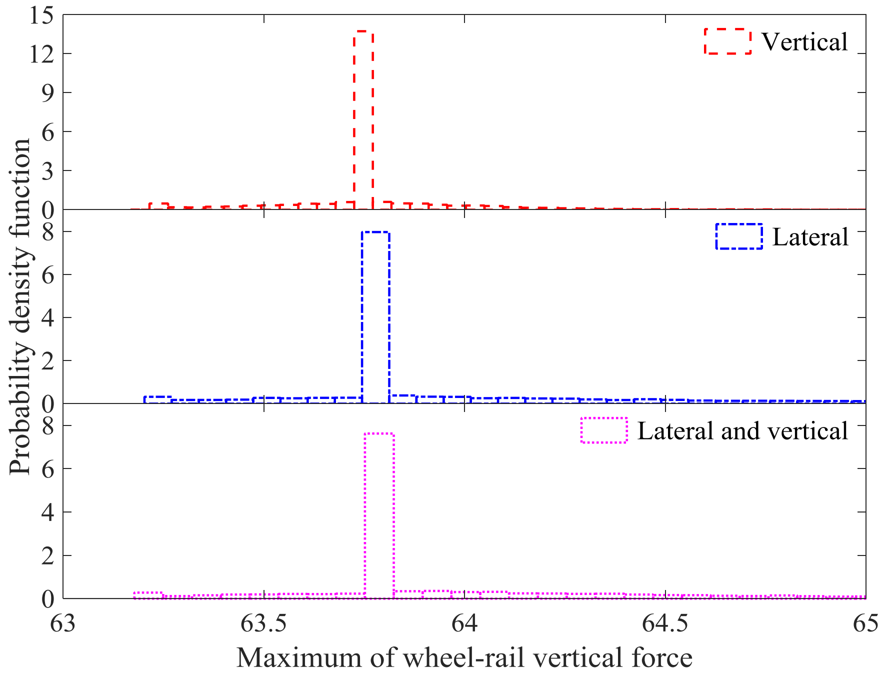

Fig. 9. Distribution of maximum wheel-rail vertical force under different seismic components

The influence of the earthquake occurrence moment on the WDC under different seismic components is given in Fig.10. It can be seen that the WDC is mainly concentrated around 0.26 under the vertical seismic component. However, the WDC is mainly concentrated in the range of 0.2~0.45 and even exceeds the limit value 0.8 in some cases, when considering the influence of the lateral seismic component. It shows that the lateral seismic component has a significant influence on the WDC. In addition, it can be seen from Fig.10 that the earthquakes have a significant influence on the train safety performance, when the first wheelset is located in the interval of 159~588m.

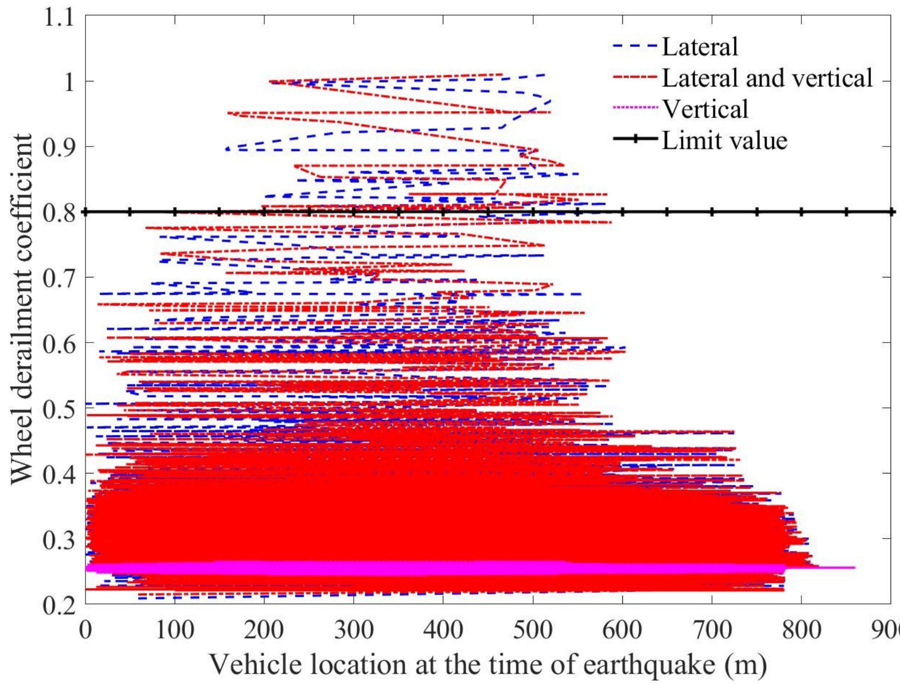

Fig. 10. Influence of earthquake occurrence moment under different seismic components

4.2 Different train running speeds

Both the lateral and the vertical seismic components are imposed. The spectrum intensity of the lateral seismic component $S_h = 7.0 \times 10^{-4}\mathrm{m}^2/\mathrm{s}^3$, and the apparent seismic wave velocity v_{app} =1000m/s. The train speeds are chosen as 80 km/h, 120 km/h, 160 km/h and 200 km/h, respectively. Under different train running speeds, the influence of earthquake occurrence moment on the safety performance of the train travelling on the bridge is studied. The FPD curves of the WDC under different train speeds are given in Fig.11. It can be seen that the running safety performance decreases with the increase of train speed. This conclusion obtained agrees well with Refs.[11,15], verifying the method used in this paper.

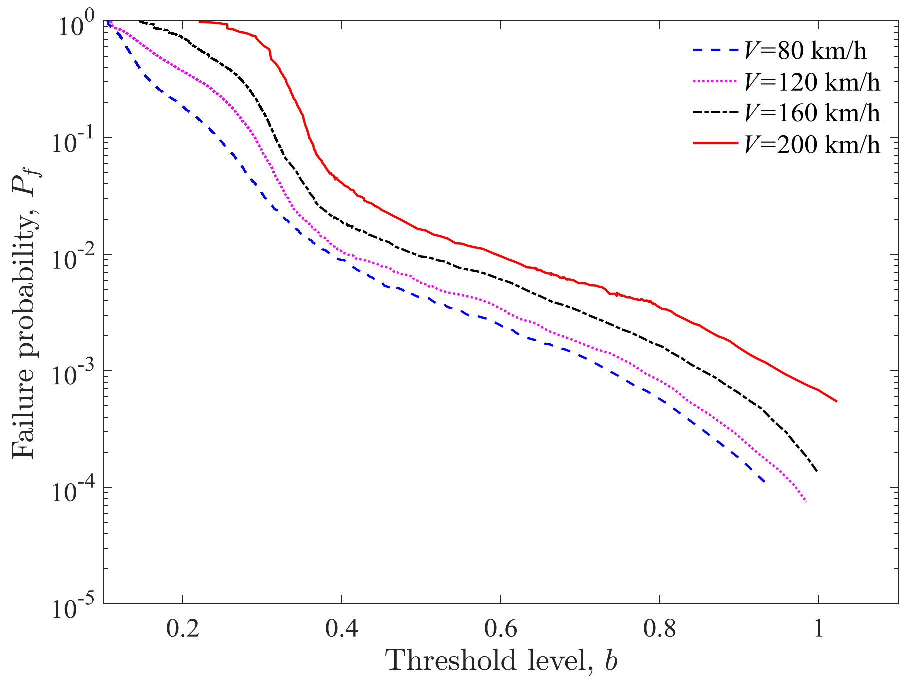

Fig. 11. FPD curves of the WDC under different running speeds

Fig.12 shows the effects of the earthquake occurrence moment on the WDC at different train speeds. The most unfavourable train position interval is 0~80 m for V =80km/h. That is, the earthquake that occurs when the first wheelset is located in the transition region between the subgrade and the bridge has a considerable impact on the train safety performance. The most unfavourable position interval for speeds of 120km/h, 160km/h and 200km/h are found to be 65~418m, 150~503m and 159~588m, respectively. It can be seen that the most unfavourable train position interval shifts along the train running direction with the increase of the train running speed. The earthquake that occurs before the train reaches $0.7L_b$ of the bridge will significantly degrade the running safety performance of the train.

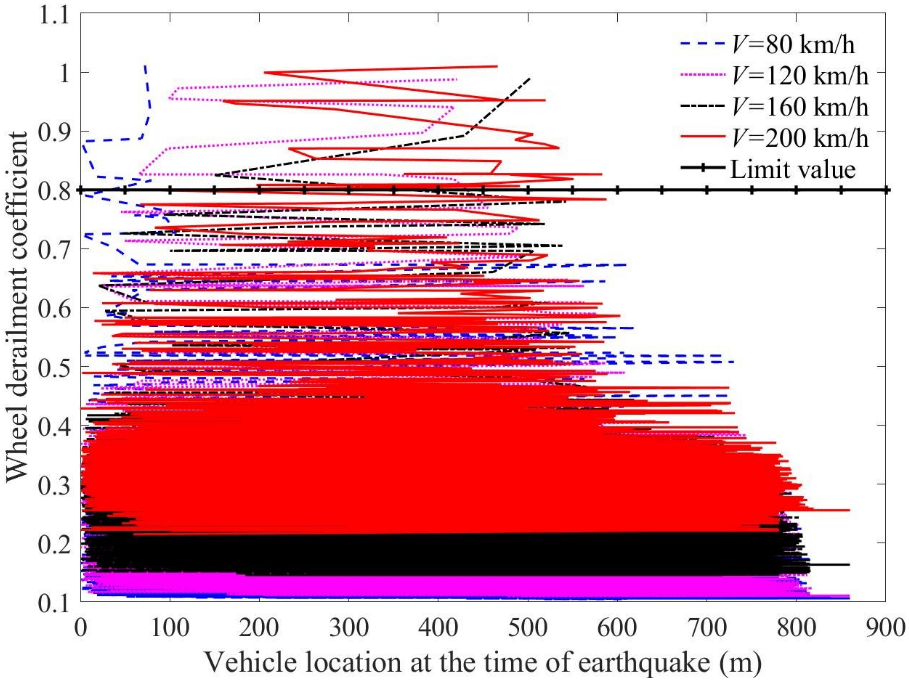

Fig. 12. Influence of earthquake occurrence moment under different running speeds

4.3 Different apparent seismic wave velocities

Both the lateral and vertical seismic components are imposed. The spectral intensity of the lateral seismic component $S_h = 7.0 \times 10^{-4}$ m^2/s^3, and the train running speed V =200km/h. The apparent seismic wave velocities are selected as 1000m/s, 1500m/s, 2000m/s and 2500m/s respectively. The influence of the earthquake occurrence moment on the safety performance of the train travelling on the bridge is studied under different apparent seismic wave velocities. Fig.13 shows the FPD curves of the WDC under apparent different wave velocities. It can be seen that for the track/bridge structure subjected to multi-point non-uniform earthquakes, the apparent seismic wave velocity has a significant impact on the train safety performance on the bridge, and the train safety performance decreases with the decrease of the seismic wave velocity. This conclusion obtained agrees well with Refs.[3,15], verifying the method used in this paper.

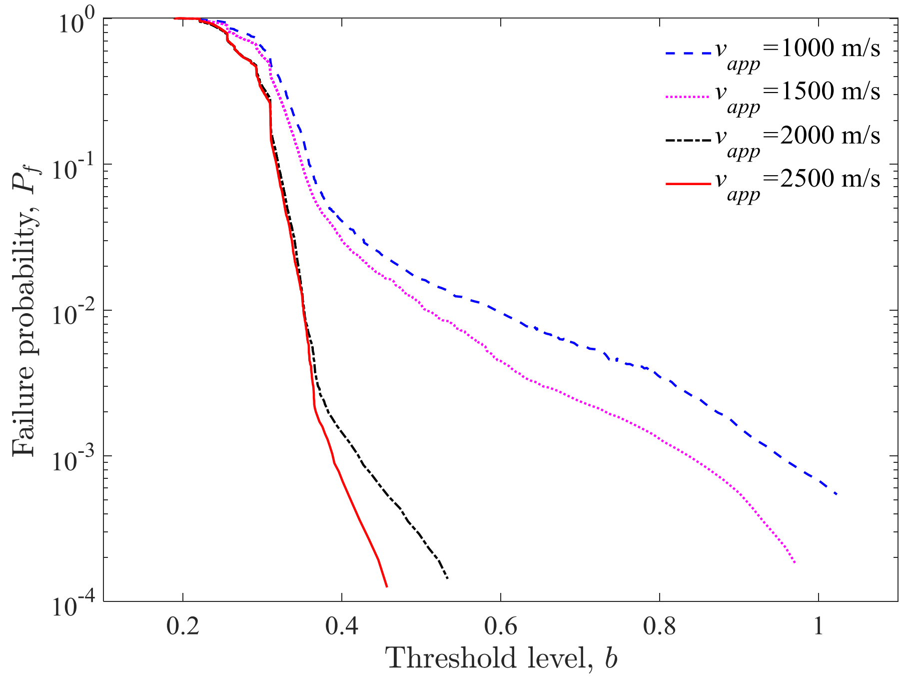

Fig. 13. FPD curves of the WDC under different apparent wave velocities

Fig. 14 shows the effects of the earthquake occurrence moment on the WDC under different apparent seismic wave velocities. At v_{app} =1000m/s, the earthquake that occurs when the first wheelset is located in the interval of 159~588m has a significant impact on the train running safety. But at v_{app} =1500m/s, the most unfavourable train position interval is 215~567m. When the apparent seismic wave velocity reaches 2000m/s or higher, the WDC is less than the limit value of 0.8, but the interval corresponding to the larger value of the WDC is 248~525m. The results show that the WDC and the range of the most unfavourable train position interval increase with the decrease of the apparent wave velocity. Under different apparent wave velocities, earthquake occurs before the train arrives at $0.7L_b$ of the bridge will significantly reduce the train safety performance.

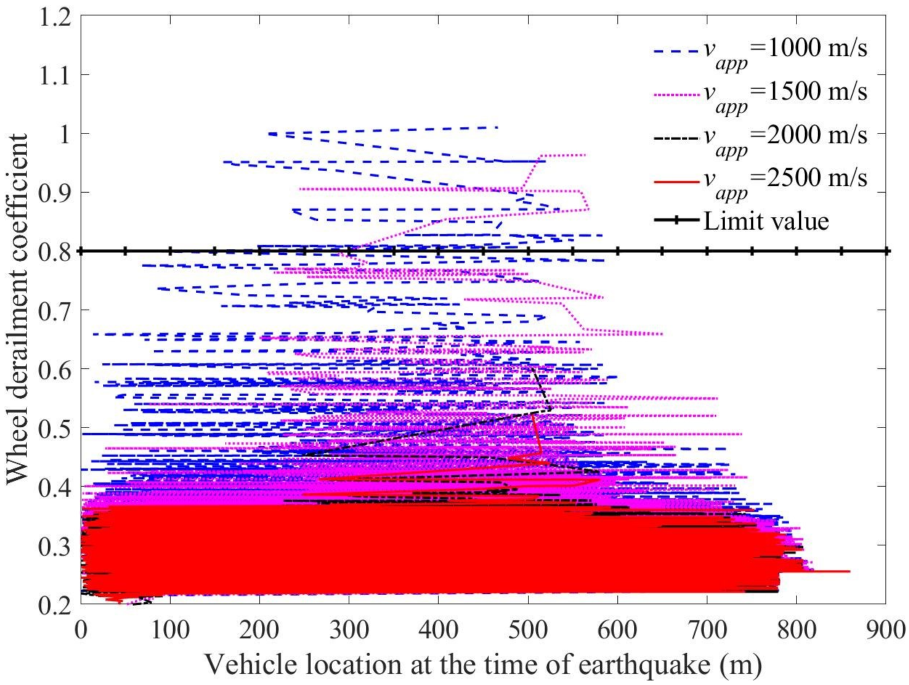

Fig. 14. Influence of earthquake occurrence moment under different apparent velocities

4.4 Different seismic intensities

Both the lateral and vertical seismic components are imposed. The apparent seismic wave velocity v_{app} =1000m/s and the train speeds takes 200 km/h. The spectral intensity of the lateral seismic component is selected as $3.0 \times 10^{-4}\,\mathrm{m^2/s^3}$, $5.0 \times 10^{-4}\,\mathrm{m^2/s^3}$, $7.0 \times 10^{-4}\,\mathrm{m^2/s^3}$ and $9.0 \times 10^{-4}\,\mathrm{m^2/s^3}$, respectively. Under different seismic intensities, the influence of the earthquake occurrence moment on the train safety performance is analysed. Fig.11 shows the FPD curves of the WDC under different seismic intensities. It can be seen that the seismic intensity has a significant impact on the train safety performance, and the safety reliability of the train running on the bridge decreases with the increase of the seismic intensity. This conclusion obtained agrees well with Ref.[14], verifying the method used in this paper.

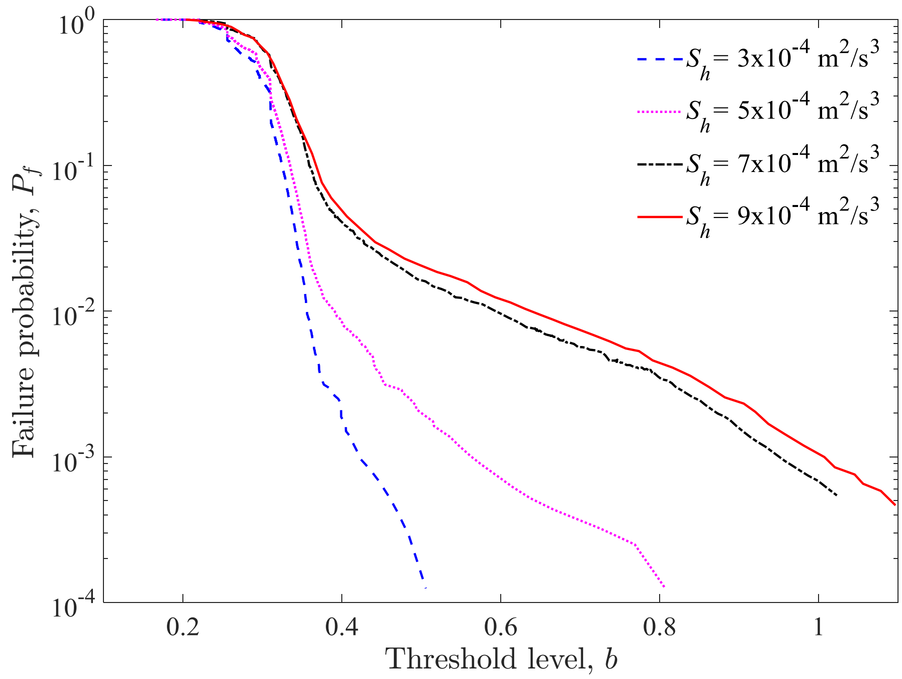

Fig. 15. FPD curves of the WDC under different seismic intensities

The effects of the earthquake occurrence moment on the WDC under different seismic intensities is given in Fig. 16. As can be seen from Fig.16 that, when $S_h = 5.0 \times 10^{-4}\mathrm{m^2/s^3}$, the earthquake that occurs when the first wheelset is located in the interval of 462~562m has a significant impact on the train running safety. The most unfavourable train position interval for seismic intensities of $7.0 \times 10^{-4} \mathrm{m}^2/\mathrm{s}^3$ and $9.0 \times 10^{-4} \mathrm{m}^2/\mathrm{s}^3$ are 159~588m and 75~590m, respectively. The results show that with the increase of seismic intensity, the WDC increases and the range of the most unfavourable train position interval also increases. Under different seismic intensities, earthquake that occurs before the train arrives at $0.7L_b$ of the bridge will significantly reduce the train safety performance.

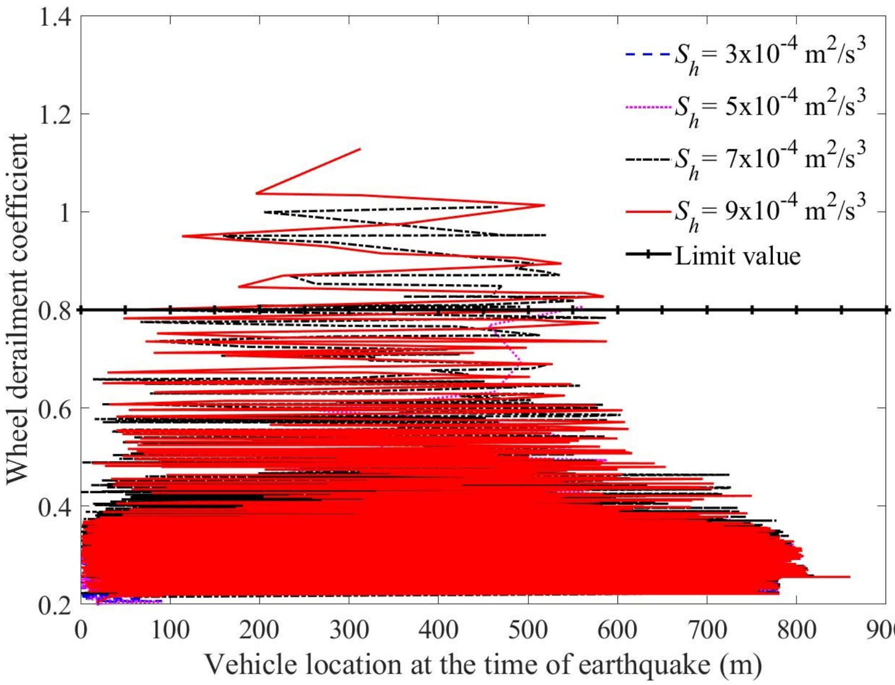

Fig. 16. Influence of earthquake occurrence moment under different seismic intensities

5 Conclusions

In this paper, the dynamic reliability of a train/track/bridge coupled system under non-stationary multi-point random seismic excitations is efficiently determined by combining the Subset Simulation method with the prediction iterative method. The computational efficiency is enhanced by improving the efficiency in computing the single sample response and reducing the number of samples required for the reliability solution. The spatial effect and the randomness of ground motion, and the randomness of train position when an earthquake occurs are considered and the influence of random multi-point earthquakes on the safety performance of a train moving on a long-span bridge is studied in term of the dynamic reliability. The dynamic models of a CRH2 high-speed train subsystem and a ballast track-continuous bridge subsystem under earthquakes are constructed separately, and a nonlinear wheel-rail contact model is established to couple the two subsystems together, in which actual wheel-rail profiles and instantaneous wheel-rail detachment can be considered. The train position at the time of the earthquake is considered a uniformly distributed random variable. Based on the cross-spectral density function matrix of seismic acceleration at each support point of the long-span bridge structure, the time-history samples of non-stationary multi-point earthquakes are generated by using the Auto Regressive Moving Average model, and inputted at the track-bridge support points in the form of displacement and velocity.

In the numerical examples, the effects of earthquake occurrence moment on the safety performance of a train moving on a long-span bridge under different seismic components, train speeds, apparent seismic wave velocities, and seismic intensities are analysed. The results show that the effect of the lateral seismic component on the wheel derailment coefficient is more significant than the vertical seismic component. With the increase of train speed, the most unfavourable train position interval shifts along the train running direction.

The range of the most unfavourable train position interval increases with the decrease of the apparent seismic wave velocity or the increase of seismic intensity. Earthquakes that occur before the train arrives at $0.7L_b$ of the bridge will significantly reduce the running safety performance of a train moving on a long-span bridge. In addition, the influence of the train speed on the WDC is greater than that of ground motion within the range of seismic parameters used in this study, by comparing the FPD curves of WDC obtained under different train speeds, different apparent seismic wave velocities or different seismic intensities.

Acknowledgments

The authors are grateful for support under grants from the National Natural Science Foundation of China (11672060, 11672052).

References

1. X. H. He, T. Wu, Y. F. Zou, Y. F. Chen, H. Guo and Z. W. Yu, Recent developments of high-speed railway bridges in China, *Struct. Infrastruct. Eng.* 13(12) (2017) 1584-1595.
2. Y. B. Yang, J. D. Yau and Y. S. Wu, *Vehicle-Bridge Interaction Dynamics-with Applications to High-Speed Railways* (World Scientific, Singapore, 2004).
3. Z. C. Zhang, Y. H. Zhang, J. H. Lin, Y. Zhao, W. P. Howson and F. W. Williams, Random vibration of a train traversing a bridge subjected to traveling seismic waves, *Eng. Struct.* 33(12) (2011) 3546-3558.
4. D. Y. Zhu, Y. H. Zhang, D. Kennedy and F. W. Williams, Stochastic vibration of the

vehicle-bridge system subject to non-uniform ground motions, *Veh. Syst. Dyn.* 52(3) (2014) 410-428.

5. Z. P. Zeng, Y. G. Zhao, W. T. Xu, Z. W. Yu, L. K. Chen and P. Lou, Random vibration analysis of train-bridge under track irregularities and traveling seismic waves using train-slab track-bridge interaction model, *J. Sound Vib.* 342 (2015) 22-43.
6. Z. P. Zeng, X. F. He, Y. G. Zhao, Z. W. Yu, L. K. Chen, W.T. Xu and P. Lou, Random vibration analysis of train-slab track-bridge coupling system under earthquakes, *Struct. Eng. Mech.* 54(5) (2015) 1017-1044.
7. H. Xia, N. Zhang and W. W. Guo, *Dynamic Interaction of Train-Bridge Systems in High-Speed Railways: Theory and Applications*/(Beijing Jiaotong University Press and Springer-Verlag GmbH Germany, Beijing and Berlin, 2018).
8. V. N. Dinh, K. D. Kim and P. Warnitchai, Dynamic analysis of three-dimensional bridge-high-speed train interactions using a wheel-rail contact model, *Eng. Struct.* 31(12) (2009) 3090-3106.
9. Y. B. Yang and Y. S. Wu, Dynamic stability of trains moving over bridges shaken by earthquakes, *J. Sound Vib.* 258(1) (2002) 65-94.
10. M. Sogabe, M. Ikeda and Y. Yanagisawa, Train-running quality during earthquakes and its improvement for railway long span bridges, *Q. Rep. RTRI.* 48(3) (2007) 183-189.
11. S. H. Ju, Nonlinear analysis of high-speed trains moving on bridges during earthquakes, *Nonlinear Dyn.* 69(1-2) (2012) 173-183.
12. Q. Zeng, and E. G. Dimitrakopoulos, Derailment mechanism of trains running over

bridges during strong earthquakes, *Procedia Eng.* 199 (2017) 2633-2638.

13. Z. B. Jin, S. L. Pei, X. Z. Li, H. Y. Liu and S. Z. Qiang, Effect of vertical ground motion on earthquake-induced derailment of railway vehicles over simply-supported bridges, *J. Sound Vib.* 383 (2016) 277-294.
14. P. A. Montenegro, R. Calçada, N. V. Pouca and M. Tanabe, Running safety assessment of trains moving over bridges subjected to moderate earthquakes, *Earthquake Eng. Struct. Dyn.* 45(3) (2016) 483-504.
15. H. Xia, Y. Han, N. Zhang and W. W. Guo, Dynamic analysis of train-bridge system subjected to non-uniform seismic excitations, *Earthquake Eng. Struct. Dyn.* 35(12) (2006) 1563-1579.
16. X. T. Du, Y. L. Xu and H. Xia, Dynamic interaction of bridge-train system under non-uniform seismic ground motion, *Earthquake Eng. Struct. Dyn.* 41(1) (2012) 139-157.
17. Y. L. Li, S. Y. Zhu, C. S. Cai, C. Yang and S. Z Qiang, Dynamic response of railway vehicles running on long-span cable-stayed bridge under uniform seismic excitations, *Int. J. Struct. Stab. Dyn.* 16(5) (2016) 1550005.
18. P. A. Montenegro, A methodology for the assessment of the train running safety on bridges, PhD thesis, University of Porto, Porto (2015).
19. Q. Zeng, and E. G. Dimitrakopoulos, Seismic response analysis of an interacting curved bridge-train system under frequent earthquakes, *Earthquake Eng. Struct. Dyn.* 45(7) (2016) 1129-1148.
20. S. K. Au and J. L. Beck, Estimation of small failure probabilities in high dimensions by

subset simulation, *Probab. Eng. Mech.* 16(4) (2001) 263-277.

21. S. K. Au, J. Ching and J. L. Beck, Application of subset simulation methods to reliability benchmark problems, *Struct. Saf.* 29(3) (2007) 183-193.
22. K. F. Tee, L. R. Khan and H. S. Li, Application of subset simulation in reliability estimation of underground pipelines, *Reliab. Eng. Syst. Saf.* 130 (2014) 125-131.
23. S. K. Au and J. L. Beck, Subset simulation and its application to probabilistic seismic performance assessment, *J. Eng. Mech.,* ASCE 129(8) (2003) 901-917.
24. C. Wetzel and C. Proppe, Stochastic modeling in multibody dynamics: aerodynamic loads on ground vehicles, *J. Comput. Nonlinear Dyn.* 5(3) (2010) 031009-031009-9.
25. W. Wang, Y. H. Zhang and H. J. Ouyang, An iterative method for solving the dynamic response of railway vehicle-track coupled systems based on prediction of wheel-rail forces, *Eng. Struct.* 151 (2017) 297-311.
26. N. Zhang and H. Xia, Dynamic analysis of coupled vehicle-bridge system based on inter-system iteration method, *Comput. Struct.* 114-115(1) (2013) 26-34.
27. Z. H. Zhu, W. Gong, L. D. Wang, Y. Bai, Z. W. Yu and L. Zhang, Efficient assessment of 3D train-track-bridge interaction combining multi-time-step method and moving track technique. *Eng. Struct.* 183 (2019) 290-302.
28. P. Antolín, N. Zhang, J. M. Goicolea, H. Xia, M. Á. Astiza and J. Oliva, Consideration of nonlinear wheel-rail contact forces for dynamic vehicle-bridge interaction in high-speed railways, *J. Sound Vib.* 332(5) (2013) 1231-1251.
29. T. Arvidsson and R. Karoumi, Train-bridge interaction - a review and discussion of key

model parameters, *Int. J. Rail Transp.* 2(3) (2014) 147-186.

30. Q. Li, Y. L. Xu and D. J. Wu, Concrete bridge-borne low-frequency noise simulation based on train-track-bridge dynamic interaction, *J. Sound Vib.* 331(10) (2012) 2457-2470.
31. K. Knothe and S. L. Grassie, Modelling of railway track and vehicle/track interaction at high frequencies, *Veh. Syst. Dyn.* 22(3-4) (1993) 209-262.
32. W. M. Zhai, Z. L. Han, Z.W. Chen, L. Ling and S. Y. Zhu, Train-track-bridge dynamic interaction: a state-of-the-art review, *Veh. Syst. Dyn.* 57(7) (2019) 984-1027.
33. H. J. Lei and J. Z. Huang, Seismic input methods in coupled system of train-track-bridge, *IOP. Conf. Ser: Earth Environ. Sci.* 153 (2018) 042007.
34. W. M. Zhai, K. Y. Wang and C. B. Cai, Fundamentals of vehicle-track coupled dynamics, *Veh. Syst. Dyn.* 47(11) (2009) 1349-1376.
35. G. Chen and W. M. Zhai, A new wheel/rail spatially dynamic coupling model and its verification, *Veh. Syst. Dyn.* 41(4) (2004) 301-322.
36. Z. L. Li, Wheel-rail rolling contact and its application to wear simulation, PhD thesis, Delft University of Technology, Delft (2002).
37. J. J. Kalker, A fast algorithm for the simplified theory of rolling contact, *Veh. Syst. Dyn.* 11(1) (1982) 1-13.
38. J. H. Lin, Y. H. Zhang, Q. S. Li and F. W. Williams, Seismic spatial effects for long-span bridges, using the pseudo excitation method, *Eng. Struct.* 26(9) (2004) 1207-1216.
39. Y. Y. Li, Y. H. Zhang and D. Kennedy, Reliability analysis of subsea pipelines under spatially varying ground motions by using subset simulation. *Reliab. Eng. Syst. Saf.* 172

(2018) 74-83.

40. E. Samaras, M. Shinzuka and A. Tsurui, ARMA representation of random processes, *J. Eng. Mech.*, ASCE 111(3) (1985) 449-461.

41. R. W. Clough and J. Penzien, *Dynamics of Structures, the 2nd edition/*(McGraw- Hill, New York, 2010).

42. C. H. Loh and Y. T. Yeh, Spatial variation and stochastic modelling of seismic differential ground movement, *Earthquake Eng. Struct. Dyn.* 16(4) (1988) 583-596.

43. J. Yang, J. B. Li and G. Lin, A simple approach to integration of acceleration data for dynamic soil-structure interaction analysis, *Soil Dyn. Earthquake Eng.* 26(8): (2006) 725-734.

44. R. A. Monzingo and T. W. Miller, *Introduction to Adaptive Arrays/*(John Wiley & Sons, New York, 1980).

45. W. M. Zhai, Two simple fast integration methods for large-scale dynamics problems in engineering, *Int. J. Numer. Methods Eng.* 39(24) (1996) 4199-4214.

46. Ministry of Railways of the People's Republic of China, No. 28 of railway transport [2008] Testing of High-speed Electric Multiple Unit on Completion of Construction, Ministry of Railways of the People's Republic of China (2008).

47. T. Miyamoto, N. Matsumoto, M. Sogabe and T. Shimomura, Railway vehicle dynamic behavior against large-amplitude track vibration, *Q. Rep. RTRI.* 45(3) (2004) 111-115.